DSN 70-Meter Antenna X- and S-Band Calibration Part I: Gain Measurements

P. H. Richter and S. D. Slobin
Telecommunications Systems Section

Aperture efficiency measurements made during 1988 on the three 70-m stations (DSS-14, DSS-43, and DSS-63) at X-band (8420 MHz) and S-band (2295 MHz) have been analyzed and reduced to yield best estimates of antenna gain versus elevation. The analysis has been carried out by fitting the gain data to a theoretical expression based on the Ruze formula. Newly derived flux density and source-size correction factors for the natural radio calibration sources used in the measurements have been used in the reduction of the data. Peak gains measured at the three stations were 74.18 (±0.10) dBi at X-band, and 63.34 (±0.03) dBi at S-band, with corresponding peak aperture efficiencies of 0.687 (±0.015) and 0.762 (±0.006), respectively. The values quoted assume no atmosphere is present, and the estimated absolute accuracy of the gain measurements is approximately ±0.2 dB at X-band and ±0.1 dB at S-band (1-σ values).

I. Introduction

Aperture efficiency measurements made on the newly completed and holographically adjusted DSN 70-m antennas at both X- and S-band were completed in the latter half of 1988. The last set of data taken was at DSS-63 after the rebolting of the major structural brace in September of that year.

Analysis of these measurements has now been completed, and a pair of gain versus elevation curves has been generated for each station at each frequency corresponding to antenna performance with and without the Earth's atmosphere under normal, clear, dry conditions.

These best estimates of antenna performance have been arrived at by fitting the data to a theoretical gain versus elevation profile based on the Ruze formula, and applying recently derived corrections to a number of natural radio source flux density and source-size correction factors used to convert source temperature measurements to aperture efficiency. These corrections have been necessitated by the publication of more recent flux density measurements for the source 3C274, especially at higher frequencies (up to 90 GHz), and the use of a new and more accurate numerical convolution procedure for calculating source-size correction factors from high-resolution radio maps.

The use of a fitting procedure based on the Ruze formula rather than the usual polynomial expansion was suggested by the somewhat unusual shapes of many of the individual gain versus elevation curves obtained at the stations. At X-band in particular, the new antennas' behavior is not easily expressed by low-order polynomials, whereas the fit to the theoretical Ruze expression is excellent. A further advantage to this method of analysis is that the fitting parameters have direct

physical significance related to the gravity-induced distortion of the main reflector, and may thus be compared with calculations based on modeling of the reflector structural performance.

The following sections of this article provide a summary of the measurements at each DSS, and describe the curve fitting and calibration procedures used to analyze these measurements and obtain best estimates of the gain characteristics for the 70-m antennas.

II. Summary of 70-m X-Band Gain versus Elevation Measurements for DSS-14, DSS-43, and DSS-63

Figures 1–3 show the gain versus elevation curves for DSS-14, -43, and -63 respectively, as measured at each station, i.e., including the effects of atmospheric attenuation. For each station, individual curves are identified according to the day of year (DOY) on which the measurements were made and the source used for the measurements. DOY refers to 1988 in all cases.

Figures 4–6 present the same set of data, except that for each curve the effects of atmospheric absorption have been removed (see Section III.A for a discussion of the procedure used).

For all cases shown in these figures, except for DSS-63 DOY 207 (source 3C274), the fit is within ±0.040 dB (1-σ), and in many cases is approximately half this value (see Appendix A for details). The data for DSS-63 taken on this date are sparse and show considerable scatter so that the 1-σ error is 0.088 dB. The curve is nevertheless included in the analysis since it provides the only comparison at this station of this important source with the more commonly used source 3C123.

It can be seen from Figs. 1–6 that there is considerable variation between the 70-m antennas, and that different sources in general give different results. On the other hand, agreement between different runs at a given station using a given source is quite good.

The question of different results for a given antenna with different sources centers on the correctness of the flux densities and source-size correction factors given in *DSN Radio Source List for Antenna Calibration*, rev. B.[1] Analysis of this question, given in Section IV, shows that as a result of the limitations inherent in previously available methods of computing the source-size correction factor, C_r, significant errors have existed in the values of both flux density S, and C_r for certain sources such as 3C274. Additionally, more recent measurements of various calibration sources at higher frequencies have resulted in a slightly revised flux density scale which results in yet another contribution to the systematic differences apparent in Figs. 1–6.

When all of these effects are taken into account, the gain versus elevation curves shown in Figs. 7 and 8 result (see Section IV.E for details). These are based on all of the data used to generate Figs. 1–6, and the fits are very good in each case (0.029 dB $< \sigma <$ 0.040 dB). Also shown in Fig. 8 is a theoretical curve based on design expectations, indicating that the actual performance at the three stations is somewhat poorer than anticipated both in terms of the maximum gain and the fall-off in gain with elevation angle [1, 4].

III. Analysis of Gain Measurements

A. Curve Fitting

As mentioned above, the gain versus elevation data for each run were fitted to a theoretical curve based on the use of the Ruze formula [2],

$$\epsilon_0(\alpha) = \epsilon_m \exp\left[-\left(\frac{4\pi\Sigma(\alpha)}{\lambda}\right)^2\right] \quad (1)$$

where

$\epsilon_0(\alpha)$ = aperture efficiency at elevation angle α

ϵ_m = maximum aperture efficiency

$\Sigma(\alpha)$ = rms half-pathlength deviation of antenna surface from best fit design surface (inches)

λ = wavelength (inches)

The rms half-pathlength deviation, $\Sigma(\alpha)$, may be expressed in terms of geometrical factors and the deviations for gravity loadings applied parallel to the reflector y- and z-axes respectively [3]

$$\Sigma^2 = S_y^2\eta^2 + S_z^2\zeta^2 + 2CS_yS_z\,\eta\zeta \quad (2)$$

where

S_y = rms half-pathlength deviation for y-axis load (α = 0 deg) (inches)

[1] *DSN Radio Source List for Antenna Calibration*, rev. B, JPL internal document D-3801, September 25, 1987. In the remainder of this article, JPL D-3801 will be used to refer to this document.

S_z = rms half-pathlength deviation for z-axis load (α = 90 deg) (inches)

$\eta = \cos\gamma - \cos\alpha$

$\zeta = \sin\gamma - \sin\alpha$

C = correlation coefficient between y- and z-axis load deviations

In the above, γ is the angle for which the aperture efficiency is maximum, so that the rms deviation Σ is relative to that at $\alpha = \gamma$.

Using Eqs. (1) and (2) the antenna gain may be expressed as

$$G_0(\alpha) = G_m + G_1 X_1(\alpha,\gamma) + G_2 X_2(\alpha,\gamma) + G_3 X_3(\alpha,\gamma) \quad (3)$$

where

$G_0(\alpha)$ = gain in dBi at elevation angle α

$G_m = G_{100} + 10\log\epsilon_m$ = maximum gain ($\alpha = \gamma$)

$G_1 = -KS_y^2$

$G_2 = -KS_z^2$

$G_3 = -2KCS_yS_z$

$X_1 = \eta^2$

$X_2 = \zeta^2$

$X_3 = \eta\zeta$

$G_{100} = 20\log(\pi D/\lambda) = 75.815$ dBi at X-band (ν = 8420 MHz)

$K = 10(4\pi/\lambda)^2\log e = 349.023$ dB/inch^2 at X-band (ν = 8420 MHz)

Equation (3) involves five parameters, G_m, G_1, G_2, G_3, and γ, and it may be used to fit the gain data at each of the stations and so determine the parameters G_m, S_y, S_z, C, and γ appropriate to each antenna. These may in turn be compared with predictions for these parameters based on theoretical models of the 70-m antenna performance.

It has been shown that predictions of 70-m antenna performance based on Geometrical Theory of Diffraction (GTD) calculations agree very well with those based on traditional ray tracing methods using the above formulation, provided the subreflector position is optimized to maximize the predicted gain [4]. Hence, the comparison referred to above should permit a good check on such theoretical calculations, within the limitations imposed by the quality of the gain measurements at each station.

In order to carry out such a comparison it was first necessary to remove any known systematic effects from the data, such as attenuation due to atmospheric absorption. Thus, the gain in the absence of an atmosphere, $G_0(\alpha)$, is related to the measured gain including atmospheric absorption, $G(\alpha)$, by the relation

$$G_0(\alpha) = G(\alpha) + \frac{A_{0_z}}{\sin\alpha} \quad (4)$$

where $G(\alpha)$ is obtained from the measured efficiency data, $\epsilon(\alpha)$,

$$G(\alpha) = 10\log\epsilon(\alpha) + 10\log\left(\frac{\pi D}{\lambda}\right)^2 \quad (5)$$

and A_{0_z}, the zenith attenuation, is calculated from an atmospheric model based on surface measurements of temperature, pressure, and relative humidity taken simultaneously with the gain measurements.

Table 1 summarizes the results of the fitting for all three stations, listing the values of γ, S_y, S_z, and C determined for each of the days indicated.

The variations in the parameters listed in Table 1 most likely arise from three different sources: random measurement errors, systematic measurement errors, and the sensitivity of the parameters themselves to small changes in the data. The latter effect is due to the fact that the fitting functions $X_j(\alpha_i)$ defined in Eq. (3), although linearly independent, are not orthogonal, i.e.,

$$\sum_{i=1}^{N} X_j(\alpha_i)\, X_k(\alpha_i) \neq 0 \qquad \text{for } j \neq k \quad (6)$$

where j,k = 1, 2, 3, and N = number of data points used in the fit [5]. This is especially significant for the correlation coefficient, which can take on a wide range of values, even changing sign as seen in the case of DSS-14 and -63, without significantly changing the goodness of the fit.

For comparison purposes, the parameter values determined from structural model calculations[2] are also listed in Table 1. These assume a value of γ = 45 deg, which is slightly different

[2] Roy Levy, personal communication.

from the fitting values listed in Table 1, so one cannot expect perfect agreement between the Table 1 and model calculation values for S_y, S_z, and C. However, small changes in the value of γ will not result in a significant change in shape if the remaining parameters remain fixed. Thus, the substantial differences actually observed between the theoretical and fitted values must be due to causes other than these small differences in γ. These could be any of those listed above, or differences between the assumed and actual antenna structure.

To illustrate the magnitude of the difference implied by the data listed in Table 1, Fig. 8 shows a comparison of the average gain curve $G_0(\alpha)$ for each station with the predictions based on the theoretical parameter values listed in the table (see Section III.E for details).

Table 2 lists the angle at which the final panel setting was carried out for each of the antennas.[3] The agreement between these values and the average of the values found in Table 1 is quite good for DSS-14 and -43, but there is about a 4-deg difference for DSS-63. The reason for this difference is not known, but it should be noted that the data for this station are more sparse than for the other stations, and show greater scatter.

It is also possible that the elevation angle used to carry out the final panel setting may not be the one for which the total rms deviation of the antenna surface from the desired figure is minimum, i.e., the setting angle may not be the value γ appearing in the Ruze formula. This is because the rms deviation includes both short-range and long-range errors, and the latter, corresponding to low-order departure from the desired shape, could, on a random basis, be of such a symmetry that the rms deviation would be reduced in magnitude at some other elevation angle as a result of gravitationally induced flexure of the structure. This new angle would then obviously be γ by definition.

The data used for DSS-63 in the above analysis were obtained prior to the rebolting of the structural brace which had previously been found to be loose enough to permit some slippage. Figure 9 shows more recent measurements compared with the average for DOY 124 and 201; this new data reflects the configuration after the rebolting of the brace. It is seen that the new data tend to fall somewhat below the previous results at low elevation angles, and that the DOY 274 data do not fit the previous data or the DOY 246 data between 20 deg and 56 deg. On the other hand, the DOY 246 data agree reasonably well with the pre-rebolting results for 25 deg $< \alpha <$ 65 deg, but tend to be somewhat high for $\alpha >$ 65 deg.

[3] Boris Seidel, personal communication.

Taken all in all, the results obtained after rebolting do not appear to indicate any significant change from the earlier results, except possibly for a lower gain at low elevation angles. However, the amount of data available and the lack of agreement between the two sets of data make it appear unwise to alter the final curve fit on the basis of these data. It appears that a systematic error is involved in the post-rebolting measurements.

B. Systematic Effects in the $\epsilon(\alpha)$ Measurements

The efficiency measurements at DSS-14 and DSS-63 show variations with elevation which in certain cases indicate the presence of systematic errors. These take the form of both periodic fluctuations and offsets; an analysis of these effects is carried out in Appendix B where it is shown that at DSS-14, for example, it appears that a small pointing error ($\Delta\phi$ = 1.2 $\times$ 10^{-3} deg) has resulted in a small average reduction in measured efficiency amounting to a 0.028-dB gain loss.

Owing to the lack of any consistent indication of such an effect at all stations for all measurements, the above loss is treated as a probable error and added to the overall error budget for the gain measurements (see Section IV.F).

IV. Calibration Analysis

A. Computation of Efficiency

The efficiency data obtained at the individual stations are derived from the measured source temperature values by means of the relation

$$\epsilon = \frac{2kTC_r}{AS} \tag{7}$$

where

k = Boltzmann's constant

T = measured source temperature

C_r = source-size correction factor

A = area of antenna = $\frac{\pi D^2}{4}$

S = source flux density

It is seen that the computed efficiency values, and hence also the gain values, depend directly on the two quantities C_r and S, which must be determined for each source used in the calibration measurements, and of course, at each fre-

quency if measurements are to be made at more than a single frequency.

Values of C_r and S used in these calculations have been taken from JPL D-3801, rev. B, and apply to the 70-m antennas at X-band. Thus, one may rewrite Eq. (7) with a more specific notation to emphasize the fact that 70-m gains are being discussed,

$$\epsilon_{70} = \frac{2kT_{70}C_{r_{70}}}{A_{70}S} \tag{8}$$

The values of S which appear in JPL D-3801 and the above equation were obtained by means of a series of measurements made using the 64-m antenna at Goldstone [6]. These measurements used Eq. (7) solved for S, but with values for the other parameters appropriate to the 64-m Goldstone antenna, i.e.,

$$S = \frac{2kT_{64}C_{r_{64}}}{A_{64}\epsilon_{64}} \tag{9}$$

where

T_{64} = measured source temperature on 64-m antenna at Goldstone

$C_{r_{64}}$ = Goldstone 64-m source-size correction factor based on Φ_B = 2.25 min = 0.0375 deg [6][4]

A_{64} = 64-m antenna area

ϵ_{64} = efficiency of 64-m antenna at Goldstone

The efficiency, ϵ_{64}, was obtained by calibrating the 64-m antenna against a single, specific source, 3C274, assuming its X-band flux density to be known

$$\epsilon_{64} = \frac{2kT_0C_{r_0}}{A_{64}S_0} \tag{10}$$

where

T_0 = measured 3C274 source temperature, 64-m Goldstone antenna

C_{r_0} = computed Goldstone 64-m correction factor for 3C274 = 1.085 ([6], and see Footnote 4)

S_0 = assumed X-band flux density for 3C274 = 46.00 Jy[5]

S_0 was taken from [7] as the best available estimate for this quantity at the time.

Combining Eqs. (8–10) one may write

$$\epsilon_{70} = \frac{2kT_{70}T_0}{A_{70}T_{64}} \times \frac{C_{r_{70}}C_{r_0}}{C_{r_{64}}S_0} \tag{11}$$

The various terms on the right-hand side of Eq. (11) are subject to errors, and the cause and influence of these are discussed in the following sections.

B. Errors in C_r

The source-size correction factor C_r corrects the measured efficiency for the loss resulting from the fact that the source has an angular extent that may not be small relative to the antenna beamwidth. Its value is determined from the relationship

$$C_r = \left(\frac{S}{\frac{S_{on}}{\Omega_0} \otimes P}\right)_{max} \tag{12a}$$

where

$$S_{on} = B \otimes P_{on} \tag{12b}$$

$$\tilde{P} = \frac{\Omega_0 \tilde{P}_n}{\tilde{P}_{on}} \tag{12c}$$

B = source brightness function

P_n = antenna relative power pattern

P_{on} = mapping antenna relative power pattern

Ω_0 = mapping antenna beam solid angle

and $\otimes$ means convolution while $\tilde{P}$ = Fourier transform of P, etc. [8].

[4] These are the values appearing in JPL D-3801, rev. A. Rev. B of this document included some corrections necessitated by beamwidth changes resulting from changes in antenna feed on the 64-m antennas.

[5] The spectral formula for 3C274 actually yields S = 46.02 Jy at ν = 8420 MHz.

The reference to a "mapping antenna" above means that the flux density map of the source, S_{on}, used to compute C_r has been obtained with an antenna whose beam solid angle $\Omega_0 << \Omega$, where the latter is the beam solid angle of the antenna being calibrated (64-m or 70-m). This insures that $\tilde{P}$, and hence P, defined by Eq. (12c) exist. Note also that

$$S = \frac{1}{\Omega_0} \int S_{on}\, d\Omega \tag{13}$$

Until recently, determinations of C_r have been based on Gaussian approximations to both the flux density map S_{on} and the antenna beams, and the computation of P by means of Eq. (12b) has been approximate and subject to error. Removal of these deficiencies has resulted in more accurate estimates of C_r for the important source 3C274 which, as seen from the discussion in Section IV.A above, plays a central role in the overall calibration process [8].

Specifically, the values of C_{r_0} and $C_{r_{70}}$ for 3C274 have been increased according to Table 3. The impact of these changes will be discussed in Section IV.D.

C. Errors in Flux Density, S

The value of S_0 = 46.00 Jy taken from [7] is based on the analysis of all of the known measurements of 3C274, as well as other important antenna calibration sources, up to the year 1974, and is computed directly from the spectral formula

$$\log S \text{ (Jy)} = a + b \log \nu \text{ (MHz)} \tag{14}$$

with $a = 5.023 \pm 0.034$ and $b = -0.856 \pm 0.010$.

The above coefficients were obtained by the authors of [7] by a least-squares fitting to data over the frequency range 400 MHz $\leqslant \nu \leqslant$ 22285 MHz, but neither the exact data used nor the exact fitting procedure employed can be determined from their paper.

More recent measurements of this source have extended the frequency range up to 90 GHz, and it becomes clear from these newer data that one cannot obtain a reasonable fit with only two coefficients. If a power law of the form

$$y = \sum_{n=0}^{3} a_n x^n \tag{15}$$

where $y = \log S$ (Jy) and $x = \log \nu$ (MHz), is used to fit the data over the entire range 400 MHz $\leqslant \nu \leqslant$ 90 GHz, then an unweighted fit results in the coefficients

$$a_0 = 3.9964$$

$$a_1 = 0.1733$$

$$a_2 = -0.3341$$

$$a_3 = 0.0352$$

with the resulting X-band value (ν = 8420 MHz) of S_0 = 45.2037 Jy.

The resulting spectrum for 3C274 is shown in Fig. 10, and a number of comments are in order regarding this and other similar results obtained by different authors.

First, the use of a power law expansion such as Eq. (15) cannot be justified on any theoretical basis. The source 3C274 for example, has a complex angular structure reflecting a complex spatial structure, and different regions of the source are known to have very different spectra [7]. Thus, total flux density measurements such as those presented by the data points shown in Fig. 10 correspond to averages over the entire source, and any simple result, as for example Eq. (14) or (15), can only mirror a fortuitous circumstance and/or inadequate resolution in frequency. This means that an accurate spectrum might require terms higher than $n = 3$, for example, but in the absence of accurate measurements at a large number of frequencies one has no way of knowing how large n must be for a best fit. Obviously, if $n = N$, the number of data points, the fit becomes perfect, but not necessarily meaningful.

A second point is illustrated by the two straight line segments shown in Fig. 10, which correspond to estimates made by Ivanov and Stankevich based on a new absolute flux scale for radio astronomy [9]. This scale uses the so-called "artificial moon" method of calibration which, according to the authors, is free of many of the problems associated with other techniques such as the use of a reference dipole or reference horn, and it is seen that it produces values that are consistently below those shown in the figure, giving S_0 = 41.96 Jy at X-band, for example.

The artificial moon method itself is open to criticism, however, and a systematic study is presently underway to resolve such discrepancies. Meanwhile, the above discussion points up some of the difficulties involved in determining S_0 for use as an absolute calibration standard. Individual flux density measurements typically have quoted errors of ±4–5 percent, to which must be added systematic errors resulting from the particular procedures used.

D. Implications of Errors in C_r and S to 70-m Antenna Calibration Results

Using primes to represent quantities for which improved estimates have recently been obtained, Eq. (11) leads to the result

$$\frac{\epsilon'_{70}}{\epsilon_{70}} = \left(\frac{C'_{r_{70}}}{C_{r_{70}}}\right)\left(\frac{C_{r_{64}}}{C'_{r_{64}}}\right)\left(\frac{C'_{r_0}}{C_{r_0}}\right)\left(\frac{S_0}{S'_0}\right) \tag{16}$$

or, in terms of the resulting change in gain,[6]

$$\Delta G = G' - G = 10 \log\left(\frac{C'_{r_{70}}}{C_{r_{70}}}\right) + 10 \log\left(\frac{C_{r_{64}}}{C'_{r_{64}}}\right) + 10 \log\left(\frac{C'_{r_0}}{C_{r_0}}\right) + 10 \log\left(\frac{S_0}{S'_0}\right) \tag{17}$$

The two main sources that were used in the 70-m antenna gain calibrations are 3C274 and 3C123, and using the above formula one can compute the correction which should be applied to the measurements obtained for each source to allow for the improved values of C_r and S.

Since the term which depends on S_0 is the same for all sources, one has for this constant contribution

$$\Delta G_{S_0} = 10 \log\left(\frac{46.00}{45.2037}\right) = 0.076 \text{ dB} \tag{18}$$

where it is assumed, in the absence of better estimates, that the curve fit to the 3C274 spectrum given by Eq. (15) is probably better than that given in [7], which was based on more limited data.

For the remaining contributions the value of ΔG is different for the two sources. For 3C274, $C_{r_{64}} = C_{r_0}$ by definition, so that

$$\Delta G_{C_r} = 10 \log\left(\frac{C'_{r_{70}}}{C_{r_{70}}}\right) = 10 \log\left(\frac{1.18}{1.106}\right) = 0.281 \text{ dB} \tag{19}$$

and hence

$$\Delta G(3C274) = 0.357 \text{ dB} \tag{20}$$

where the values for $C_{r_{70}}$ have been taken from Table 3.

For 3C123 no new computations of $C_{r_{64}}$ or $C_{r_{70}}$ have yet been made, but since this source is well represented by a pair of closely spaced Gaussian distributions, and the value of C_r is not large, any corrections ought to be small. Thus, in the absence of information to the contrary one can assume no change in $C_{r_{64}}$ or $C_{r_{70}}$ so that

$$\Delta G_{C_r} = 10 \log\left(\frac{C'_{r_0}}{C_{r_0}}\right) = 10 \log\left(\frac{1.15}{1.085}\right) = 0.253 \text{ dB} \tag{21}$$

and hence

$$\Delta G(3C123) = 0.329 \text{ dB} \tag{22}$$

In addition to 3C274 and 3C123, a limited number of measurements were made using sources 3C161 and 3C218. The former is small enough to be considered a point source, so here also there should be no change in $C_{r_{64}}$ or $C_{r_{70}}$; thus ΔG for this source should be the same as that for 3C123,

$$\Delta G(3C161) = 0.329 \text{ dB} \tag{23}$$

Source 3C218, on the other hand, is an extended source, so that in the absence of newly determined values for $C_{r_{64}}$ and $C_{r_{70}}$ it is impossible to determine a ΔG value for this source. Thus, no attempt has been made to use the efficiency measurements obtained with it.

The source 0521-365 is variable so that data on $\epsilon(\alpha)$ obtained with this source can be used to determine the shape of the gain curve, but not its absolute level. Fortunately, data were also taken using 3C274 at DSS-43, where 0521-365 was used, and hence, an absolute calibration of this antenna is possible.

The procedure used was to average the two $G_0(\alpha)$ curves obtained with 0521-365, average the two curves obtained with 3C274, and then determine the average difference between these two over the range of elevation angles for which they overlap (13 deg $< \alpha <$ 42 deg). This difference was then combined with the ΔG value for 3C274 to obtain a corresponding correction for 0521-365,

$$\Delta G(0521\text{-}365) = 0.305 \text{ dB} \tag{24}$$

[6]These expressions consider changes resulting from improved estimates of C_r and S, and do not take into account either the probable errors of such estimates, or errors in the measured temperatures appearing in Eq. (11). These are discussed in Section IV.F.

When the above corrections are applied to the individual runs at each of the 70-m stations, the gain curves shown in Figs. 11–16 are obtained, and it is seen that the spread between curves has been reduced and the overall gains increased.

In the following sections final estimates for the gain curves at each station are obtained, and an assessment is made of the probable errors involved in terms of the analysis made above.

E. Estimates of Gain versus Elevation for Individual 70-m Stations

The average gain characteristic for each DSS has been obtained by applying the corrections of Eqs. (20), (22), (23) and (24) to the data for each run at a given station, and then determining the best fit of the combined data sets to Eq. (3), as was previously done for each individual run (see Appendix A for a discussion of the quality of the fits).

For DSS-14 all six data sets have been used, while for DSS-43 and DSS-63 only the two sets each obtained with sources 0521-365 and 3C123, respectively, have been used.

The results of this final curve fitting are shown in Figs. 7 and 8, and Table 4 lists the fitting parameters for the three stations, together with the theoretical values shown in Table 1, and the design-expected peak gain [1]. The error estimates listed in the table for the measured peak gains G_m are based on the analysis carried out in the following section.

F. Estimates of Errors in Aperture Efficiency and Gain

From Eq. (7) one may express the variance of the efficiency, σ_ϵ^2, as

$$\left(\frac{\sigma_\epsilon}{\epsilon}\right)^2 = \left(\frac{\sigma_T}{T}\right)^2 + \left(\frac{\sigma_{C_r}}{C_r}\right)^2 + \left(\frac{\sigma_s}{S}\right)^2 \tag{25}$$

where

σ_T^2 = variance of measured source temperature

$\sigma_{C_r}^2$ = variance of source-size correction factor

σ_s^2 = variance of source flux density

The measured source temperature variance, σ_T^2, itself depends on many factors, not all of which can be accurately estimated. However, if one considers the measurements made at a given station and with a given source, then the last two terms in Eq. (25) vanish, so that

$$\left(\frac{\sigma_T}{T}\right)^2 = \left(\frac{\sigma_\epsilon}{\epsilon}\right)^2\Bigg|_{\substack{\text{station,}\\ \text{source}}} \tag{26}$$

Examination of the data taken at all three stations shows that σ_ϵ^2 is comparable for each if one considers individual runs (see Figs. A-1–A-11). When all runs at a given station are considered, however, the variation is larger at DSS-14 than at the other two, and using this larger value as a conservative estimate, one obtains

$$\frac{\sigma_T}{T} = \frac{\sigma_\epsilon}{\epsilon}\Bigg|_{\substack{\text{DSS14}\\ \text{3C123}}} = 0.010 \tag{27}$$

The remaining terms in Eq. (25) must be considered from the point of view of ensemble averages, and are estimated by

$$\frac{\sigma_{C_r}}{C_r} = 0.020$$
$$\frac{\sigma_s}{S} = 0.040 \tag{28}$$

the former being based on source-map and beamwidth accuracies [8], and the latter on quoted errors in the literature on source flux density measurements [7].[7]

Combining the above

$$\frac{\sigma_\epsilon}{\epsilon} = 0.046 \tag{29}$$

resulting in a corresponding gain error of

$$\sigma_G = {}^{+0.19}_{-0.20}\ \text{dB} \tag{30}$$

If the estimated pointing loss found in Appendix B (0.028 dB) is added to the upper bound above, then the error estimate becomes

$$\sigma_G = \pm 0.21\ \text{dB} \tag{31}$$

[7]As mentioned earlier in this article, such errors are typically 4–5 percent. The smaller value is chosen because of a small degree of confidence stemming from the relative insensitivity of S_0 to various curve fits to the 3C274 spectral data.

V. Summary of 70-m S-Band Gain versus Elevation Measurements for DSS-14, DSS-43, and DSS-63

Compared with the X-band measurements, only a limited amount of data were gathered at the three DSSs at S-band. At DSS-14 only a single run was made, at DSS-43 three were made, and at DSS-63 two were made. Fortunately, the data at DSS-14 cover the range of elevation angles from α = 7 deg to α = 84 deg with the calibration source 3C123, while at DSS-43 the full range measurements with the variable source 0521-365 (10 deg $< \alpha <$ 85 deg) are complemented by limited range data obtained with the calibration sources 3C274 and 3C218, thus permitting an absolute gain calibration of both stations in a manner similar to that employed in the X-band analysis.

At DSS-63 neither of the runs is suitable for analysis owing to the large amount of scatter present in the measurements, and consequently no attempt has been made to determine the S-band gain characteristics for this station directly.

However, as described below (see Section VI), it has nonetheless been possible to obtain a calibrated gain curve for this station at S-band by making limited use of the S-band data and combining this with the X-band results for the same station.

The results of the analysis of DSS-14, DSS-43, and DSS-63 data are summarized in Figs. 17 and 18, which show $G(\alpha)$ and $G_0(\alpha)$ respectively for each of these stations. As in the case of the X-band results, these curves represent the result of fitting to the Ruze formula and applying overall gain corrections resulting from updated C_r and S values obtained for S-band. The details of this analysis are given in the following sections.

VI. Analysis of S-Band Gain Measurements

Figures 19 and 20 show the results of fitting Eq. (3) to the measured data for DSS-14 and -43, using Eqs. (4) and (5) to transform $\epsilon(\alpha)$ into $G(\alpha)$ and $G_0(\alpha)$ as before, where for S-band (ν = 2295 MHz), K = 25.9296 dB/in.^{2}, and for all stations the single value A_{0_z} = 0.0297 has been used.

It is seen that the gain curves are very flat, as expected, thus making the estimate of the angle γ obtained from such a fit ambiguous. For this reason γ has been fixed at the values determined from the X-band fitting procedure for each of the two stations, and the S-band fits are obtained using only the four remaining parameters G_m, S_y, S_z, and C.

The DSS-43 curve is also seen to be anomalously low owing to the choice of an abnormally high assumed flux density value for the variable source 0521-365 in computing $\epsilon(\alpha)$ from $T(\alpha)$ via Eq. (7). The absolute calibration of the S-band gains is discussed in the following section.

Comparison of the parameter values S_y and S_z obtained at X-band and at S-band for DSS-14 and -43 shows that there is reasonably good agreement in general, although the S-band values for DSS-43 appear somewhat higher than the corresponding X-band values for this station. However, by virtue of the flatness of the curves, the same ambiguity referred to above for the angle γ also exists to a considerable extent for the parameters S_y, S_z, and C, i.e., different combinations of these parameters will provide essentially the same $G_0(\alpha)$ curve within the experimental accuracy of the measurements.

In view of this it is of interest to see how well the S-band data are fit by the X-band parameters γ, S_y, S_z, and C. In principle, these ought to be the same at both frequencies, as the latter three depend only on how the antenna structure distorts as its elevation is changed from the value γ, which is itself, of course, a fixed quantity.

Such a comparison is made in Figs. 21 and 22, which show curves generated with the X-band parameters superimposed on the $G(\alpha)$ data points measured at S-band. The fits were obtained by adjusting the single remaining parameter G_m, the maximum gain, and it is seen from these figures that the resulting fits are very good. The σ values for the best fits to the S-band data, σ_{ss}, and the X-band parameter fits to the S-band data, σ_{xs}, are compared in Table 5, and it is seen that the latter are only slightly larger than the former, both being very small.

Since there is little to choose between the two fitting procedures considered above, and since the four-parameter set γ, S_y, S_z, C should be frequency independent, the X-band parametric fits to the S-band data are chosen as the final representations for the shape of the S-band gain curves for DSS-14 and -43.

While the DSS-63 data are not suitable for direct determination of the gain characteristics for this station, as mentioned in Section V, that taken on DOY 124 yield a maximum gain G_m which is very close to that found for the other two stations. This value of G_m, adjusted for calibration errors as discussed in Section VII, has been combined with the remaining X-band parameters for this station to determine its absolute S-band gain curve, once again taking advantage of the frequency-independent nature of these parameters. The results of this determination are shown in Figs. 17 and 18, and the fit to the S-band data from which the value of G_m is estimated is shown in Fig. 23.

VII. S-Band Calibration Analysis

Determination of the absolute maximum gains, G_m, for each of the three DSSs at S-band follows the same procedure described in Section IV, where newly determined values for the source flux densities, S, and source-size correction factors, C_r, are used to correct the measured gain values discussed in the previous section.

The analysis in Section IV follows exactly the same way for S-band, except that the 26-m station at DSS-13 was used in determining the S-band D-3801 values for S and C_r, rather than the 64-m station. These determinations were made by Klein and Stelzried [10] by essentially the same procedure that was later used by Turegano and Klein [6] at X-band, using source 3C274 as a standard to calibrate secondary standards, including 3C123 and 3C218.

One difference occurs at S-band however, and this is that the flux density assumed for 3C274 during the 26-m calibration measurements was not the same as that appearing in D-3801, as was the case at X-band. The reason for this difference is that at the time the 26-m measurements were made, the best estimate of this quantity was that due to Baars and Hartsuijker [11], namely S = 140.3 Jy, whereas at the time of writing D-3801 rev. A (June 30, 1987), the best estimate was that determined by Baars, Genzel, Pauliny-Toth, and Witzel, S = 140.00 Jy [7]. This value remained the same in D-3801 rev. B, and hence is the one used in determining S-band gains using the source 3C274.

As a matter of interest, yet another value for this quantity was determined by direct, absolute measurements using a calibrated horn reference by Freiley, Batelaan, and Bathker [12]. These authors obtained the value S = 136.5 ± 2.6 Jy, which is significantly lower than the above values.[8]

The power law fit of Eq. (15) yields an S-band value (ν = 2295 MHz) of 138.48 Jy, which is between the Baars et al. [7] estimate and that of Freiley et al. [12]. Given the tolerances for these measurements it seems reasonable to use the above value of 138.48 Jy and so maintain consistency with the X-band analysis, and this is done below.

As a consequence of the above-mentioned difference between the 3C274 S value used in D-3801 rev. B and that used by Klein and Stelzried, the ΔG values computed for 3C274 on the one hand, and 3C123 and 3C218 on the other, are different, i.e.,

$$\Delta G_{s_0}\,(3C274) = 10 \log \left(\frac{140.00}{138.48}\right) = 0.047 \text{ dB} \quad (32)$$

$$\Delta G_{s_0}\,(3C123/3C218) = 10 \log \left(\frac{140.3}{138.48}\right) = 0.057 \text{ dB} \quad (33)$$

Table 6 summarizes the results of recomputing the 3C274 26-m C_r values, C_{r_0}, and the 70-m C_r values, $C_{r_{70}}$, at S-band [8]. From these values the following ΔG_{C_r} values are readily obtained:

$$\Delta G_{C_r}\,(3C274) = 10 \log \left(\frac{1.205}{1.14}\right) = 0.241 \text{ dB} \quad (34)$$

$$\Delta G_{C_r}\,(3C123/3C218) = 10 \log \left(\frac{1.045}{1.035}\right) = 0.042 \text{ dB} \quad (35)$$

Combining these

$$\Delta G\,(3C274) = 0.288 \text{ dB} \quad (36)$$

$$\Delta G\,(3C123/3C218) = 0.099 \text{ dB} \quad (37)$$

In the above it has been assumed that, owing to the very small values of C_r for the 26-m and 70-m antennas for both 3C123 and 3C218, no significant changes in these values would occur as a result of recomputation.

When average differences are determined from gain measurements made at DSS-43 using the three sources 0521-365, 3C274, and 3C218, it is found that

$$G\,(3C218) - G\,(3C274) = 0.192 \text{ dB} \quad (38)$$

This should be equal to

$$\Delta G\,(3C274) - \Delta G\,(3C218) = 0.190 \text{ dB} \quad (39)$$

and it is seen that the agreement is excellent.

Combining these gain corrections with the measured gain using 0521-365, the gain correction for this source is found to be

$$\Delta G\,(0521\text{-}365) = 2.395 \text{ dB} \quad (40)$$

As mentioned above, this large value is the result of the use of an abnormally high flux density value for the efficiency calculations made at the station.

When the above gain corrections are applied to the curve fits obtained for each station, the G_m values listed in Table 7 are found.

[8] The frequency used by these authors was 2278.5 MHz. If their flux density is translated to 2295 MHz using the Baars, et al. [7] spectral index of −0.856, the result is another 0.6 percent lower.

According to the design estimates of Bathker and Slobin [1], the 70-m S-band peak gains should lie in the range 63.27–63.35 dBi, so the agreement between these estimates and the measured values is excellent.[9]

The error estimates included in Table 7 are based on an analysis similar to that described in Section IV.F, where the individual error contributions are

$$\frac{\sigma_T}{T} = 0.035$$

$$\frac{\sigma_{C_r}}{C_r} = 0.015 \tag{41}$$

$$\frac{\sigma_S}{S} = 0.02$$

so that

$$\frac{\sigma_\epsilon}{\epsilon} = 0.025$$

$$\sigma_G = \pm 0.11 \text{ dB} \tag{42}$$

The 2-percent error estimate for S-band flux density is based on the very careful work of Freiley et al. [12], plus the fact that the new value for S obtained by the curve fitting procedure described in Section IV.C is within 2 percent of both their estimate and that due to Baars et al. [7].

VIII. Summary and Conclusions

The final curve fits to the X-band data (Fig. 8) indicate that there are distinct differences between the gain characteristics of the three DSS 70-m antennas. The highest peak gain is achieved by DSS-63 (G_m = 74.29 dBi at γ = 47.7 deg), while the flattest characteristic, and that most closely approximating the theoretical performance, occurs at DSS-14.

Comparison of the peak gains listed in Table 4 with the design-expected performance reported by Bathker and Slobin [1], $G_m = 74.32^{+0.05}_{-0.14}$ dBi, shows that the two are consistent when allowance is made for the probable errors in both cases, i.e., the upper bounds of the Table 4 values exceed the lower bound of 74.18 dBi for the design expectations.

The situation with respect to the actual shapes of the gain curves, however, is less satisfactory. The three antennas show distinctly different behavior, and only one, DSS-14, is in good agreement with predictions based on structural model calculations.[10]

If the measured curve shown in Fig. 8 for DSS-14 is displaced upward to coincide with the theoretical curve at the peak, the two virtually lie on top of one another for 10 deg $\leqslant \alpha \leqslant$ 60 deg, and the maximum difference between them is 0.26 dB at α = 90 deg. However, if the same thing is done for DSS-63, discrepancies amounting to 0.5 to 0.6 dB exist at low and high elevations respectively. For DSS-43 these differences amount to 0.5 dB at each end.

Based on estimates of the probable measurement errors inherent in the characteristics shown in Fig. 8, it seems unlikely that these discrepancies are measurement related, especially since the three antennas behave quite differently from one another.

The relatively good agreement found between calculated and measured peak gains, on the other hand, has been achieved as a consequence of improved estimates of source flux densities and source-size correction factors for the natural radio sources used to calibrate the antennas [8]. Here, corrections on the order of 0.3 dB have brought the measured gains to within 0.15 dB of the theoretical value, on the average.

[9] These authors' analysis was carried out assuming a frequency of 2285 MHz, so their gain results have been translated to 2295 MHz under the assumption that the aperture efficiency is sensibly constant over this small range.

[10] Roy Levy, personal communication.

Acknowledgments

The authors would like to thank Dan Bathker, Michael Klein, and Roy Levy for their continued interest in the analysis presented in this article, and their very helpful criticism regarding several important points discussed. Thanks are also due to Timothy Pham for his assistance in carrying out the curve fitting and producing the figures for the article, and last but not least, to Ted Peng for his encouragement and patience in seeing the work to its completion.

References

[1] D. A. Bathker and S. D. Slobin, "DSN 70-M Antenna Microwave Optics Design and Performance Improvements Part I: Design Optimization," *TDA Progress Report 42-97*, Jet Propulsion Laboratory, Pasadena, California, this issue.

[2] J. Ruze, "Antenna Tolerance Theory—A Review," *Proc. IEEE*, vol. 54, no. 4, pp. 640–663, April 1966.

[3] R. Levy, "A Method for Selecting Antenna Rigging Angles to Improve Performance," *Space Programs Summary 37-65*, vol. II, Jet Propulsion Laboratory, Pasadena, California, pp. 72–76, September 30, 1970.

[4] J. M. Schredder, "Seventy-Meter Antenna Performance Predictions: GTD Analysis Compared with Traditional Ray-Tracing Methods," *TDA Progress Report 42-92*, vol. October–December, Jet Propulsion Laboratory, Pasadena, California, pp. 166–174, February 15, 1988.

[5] P. R. Bevington, *Data Reduction and Error Analysis for the Physical Sciences*, New York: McGraw-Hill, p. 144, 1969.

[6] J. A. Turegano and M. J. Klein, "Calibration Radio Sources for Radio Astronomy: Precision Flux Density Measurements at 8420 MHz," *Astron. Astrophys.*, vol. 86, pp. 46–49, 1980.

[7] J. M. W. Baars, R. Genzel, I. I. K. Pauliny-Toth, and A. Witzel, "The Absolute Spectrum of Cas A; An Accurate Flux Density Scale and a Set of Secondary Calibrators," *Astron. Astrophys.*, vol. 61, pp. 99–106, 1977.

[8] M. J. Klein and P. H. Richter, "Accurate Radio Astronomy Correction Factors C_r for Extended Sources," to be submitted to the *TDA Progress Report*.

[9] V. P. Ivanov and K. S. Stankevich, "Absolute Flux Scale for Radioastronomy (Review)," *Izvestiya Vysshikh Uchebnykh Zavedenni, Radiofizika*, vol. 29, no. 1, pp. 3–27, January 1986.

[10] M. J. Klein and C. T. Stelzried, "Calibration Radio Sources for Radio Astronomy: Precision Flux-Density Measurements at 2295 MHz," *Astron. J.*, vol. 81, no. 12, pp. 1078–83, 1976.

[11] J. M. W. Baars and A. P. Hartsuijker, "The Decrease of Flux Density of Cassiopeia A and the Absolute Spectra of Cassiopeia A, Cygnus A, and Taurus A," *Astron. Astrophys.*, vol. 17, pp. 172–181, 1972.

[12] A. J. Freiley, P. D. Batelaan, and D. A. Bathker, "Absolute Flux Density Calibrations of Radio Sources: 2.3 GHz," JPL Technical Memorandum 33-806, Jet Propulsion Laboratory, Pasadena, California, p. 4-12, December 1, 1977.

Table 1. Ruze-Levy X-band fitting parameters obtained from individual runs at the three 70-m stations; theoretical values calculated by Levy are also shown for comparison

DSS	DOY	γ, deg	S_y, in.	S_z, in.	C
14	100	42.76	0.075	0.063	0.855
14	101	47.32	0.083	0.078	0.775
14	109	41.27	0.121	0.119	0.964
14	114	46.21	0.049	0.022	−0.997
14	115/116	46.74	0.092	0.075	0.650
14	143	48.31	0.074	0.040	0.152
43	192/193	47.73	0.074	0.087	0.389
43	193/194	44.68	0.053	0.079	0.096
63	124	46.96	0.132	0.133	0.820
63	201	48.20	0.059	0.048	−0.820
63	207	42.95	0.059	0.046	−0.970
Theoretical Values		45.00	0.032	0.041	0.030

Table 2. Holographic setting angles for the three 70-m antennas

DSS	Setting angle, deg
14	47.0
43	47.3
63	41.8

Table 3. Comparison of old and new source-size correction factors for source 3C274 with the 64-m antennas (C_{r_0}) and the 70-m antennas ($C_{r_{70}}$) at X-band

	Old value	New value
C_{r_0}	1.085	1.15
$C_{r_{70}}$	1.106	1.18

Table 4. Final Ruze-Levy X-band parameter fits for the three 70-m antennas based on overall averages of calibrated data

DSS	γ, deg	G_m, dB	S_y, in.	S_z, in.	C
14	45.930	74.172 ± 0.21	0.0462	0.0209	−0.9935
43	46.155	74.092 ± 0.21	0.0665	0.0857	0.3255
63	46.836	74.284 ± 0.21	0.0645	0.0702	−0.0300
Theoretical Values	45.000	$74.32\ ^{+0.05}_{-0.14}$	0.032	0.041	0.030

Table 5. Comparison of the standard deviations for fitting S-band data with X-band and S-band Ruze-Levy parameters

DSS	σ_{xs}, dB	σ_{ss}, dB
14	0.015	0.012
43	0.017	0.015

Table 6. Comparison of old and new source-size correction factors for source 3C274 with the 26-m antenna (C_{r_0}) and the 70-m antennas ($C_{r_{70}}$) at S-band

	Old value	New value
C_{r_0}	1.035	1.045
$C_{r_{70}}$	1.14	1.205

Table 7. Final S-band peak gains (no atmosphere) for the three 70-m antennas

DSS	G_m, dB
14	63.301 ± 0.11
43	63.354 ± 0.11
63	63.361 ± 0.11

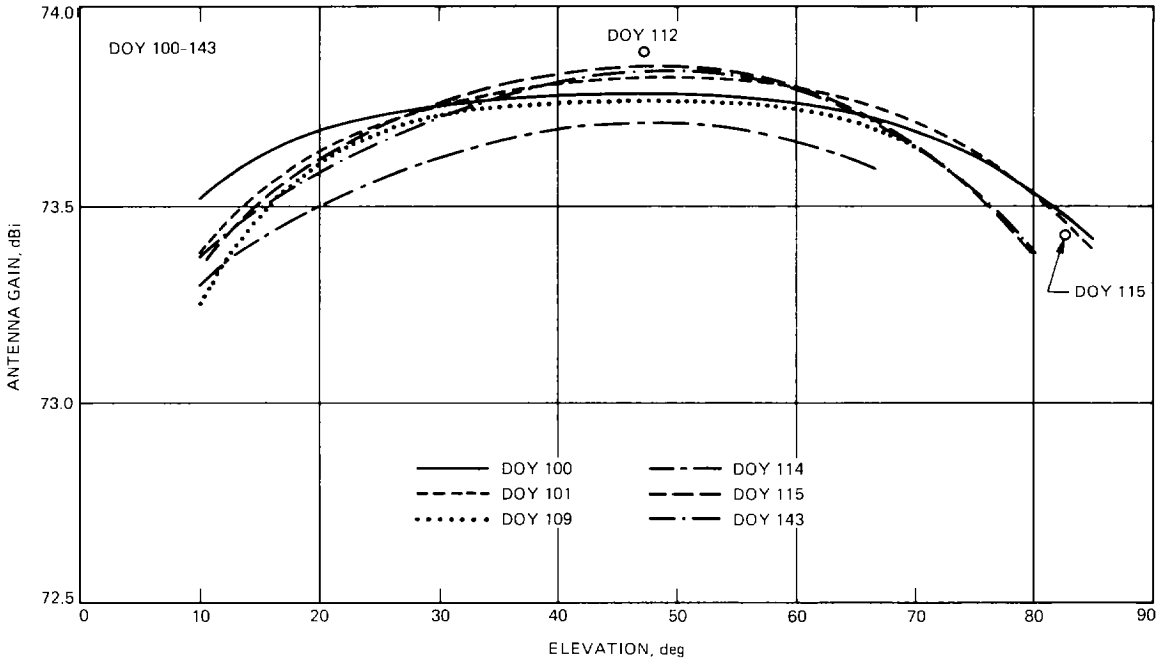

Fig. 1. X-band gain versus elevation for the 70-m antenna at DSS-14 based on uncalibrated data and including atmospheric absorption.

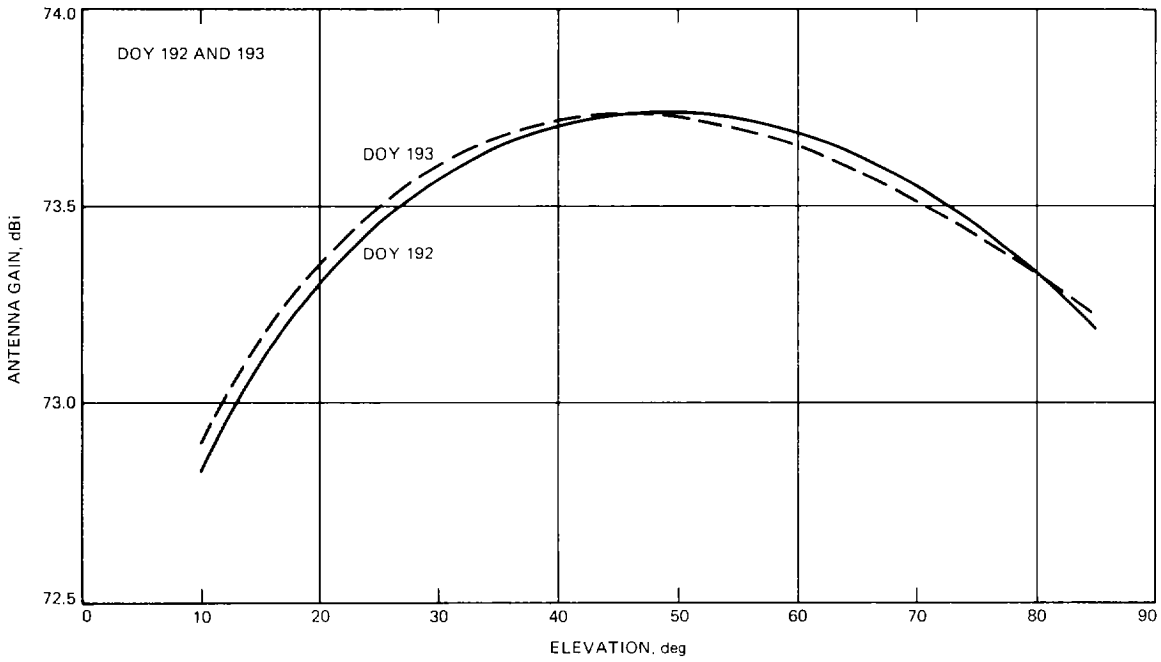

Fig. 2. X-band gain versus elevation for the 70-m antenna at DSS-43 based on uncalibrated data and including atmospheric absorption.

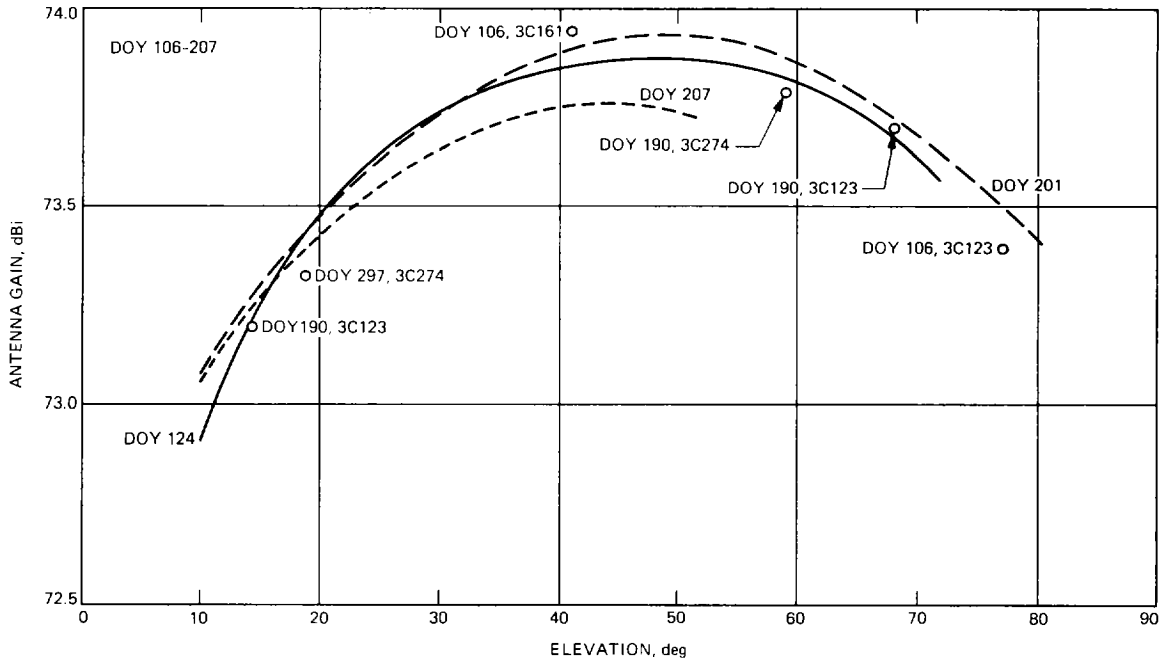

Fig. 3. X-band gain versus elevation for the 70-m antenna at DSS-63 based on uncalibrated data and including atmospheric absorption.

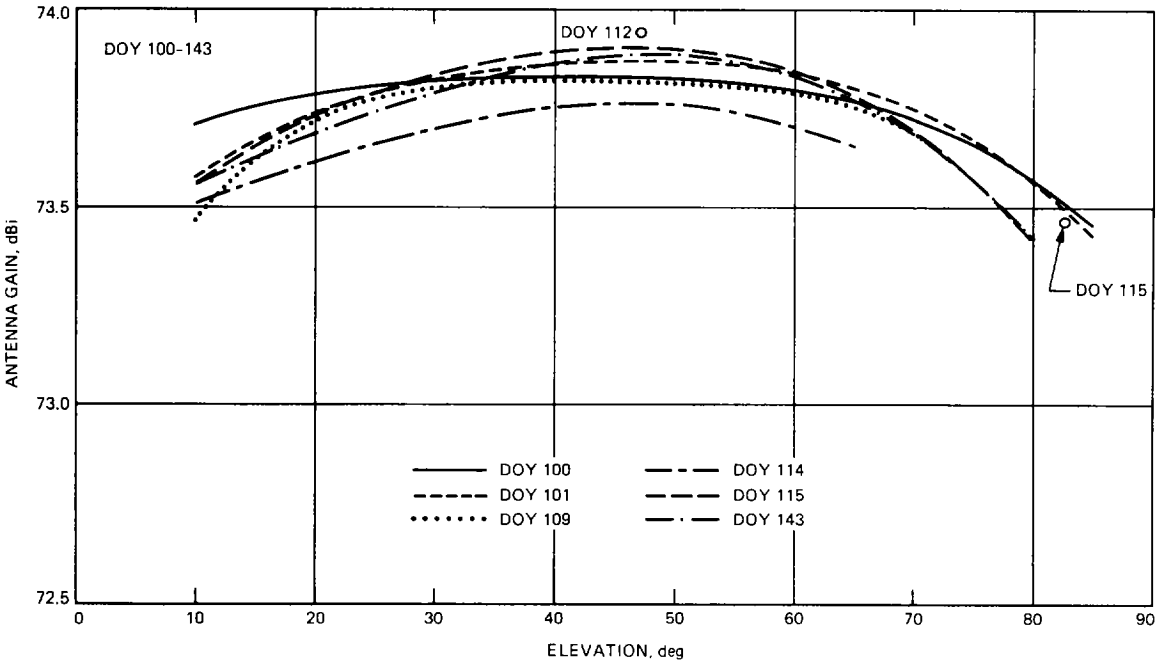

Fig. 4. X-band gain versus elevation for the 70-m antenna at DSS-14 based on uncalibrated data. Atmospheric absorption has been removed.

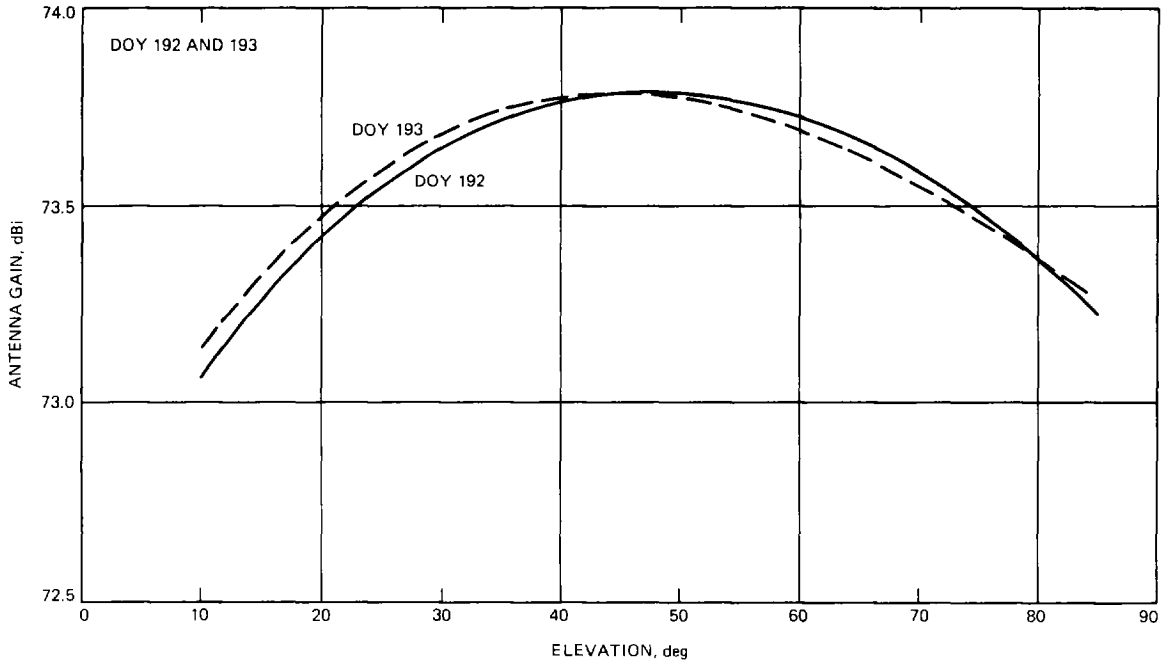

Fig. 5. X-band gain versus elevation for the 70-m antenna at DSS-43 based on uncalibrated data. Atmospheric absorption has been removed.

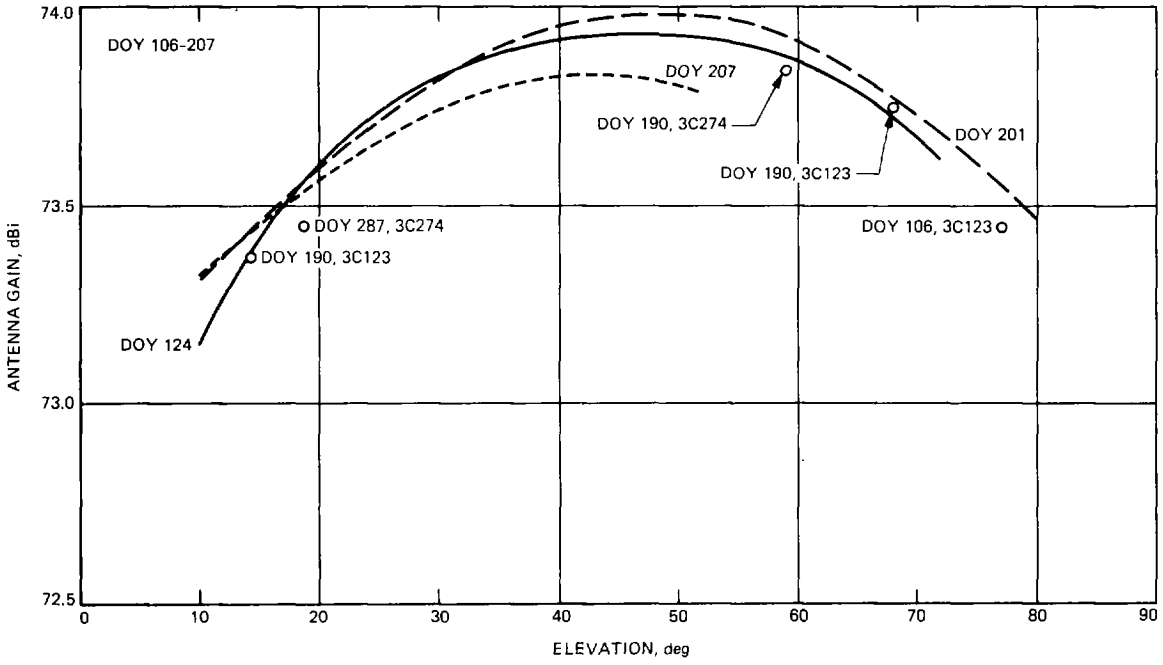

Fig. 6. X-band gain versus elevation for the 70-m antenna at DSS-63 based on uncalibrated data. Atmospheric absorption has been removed.

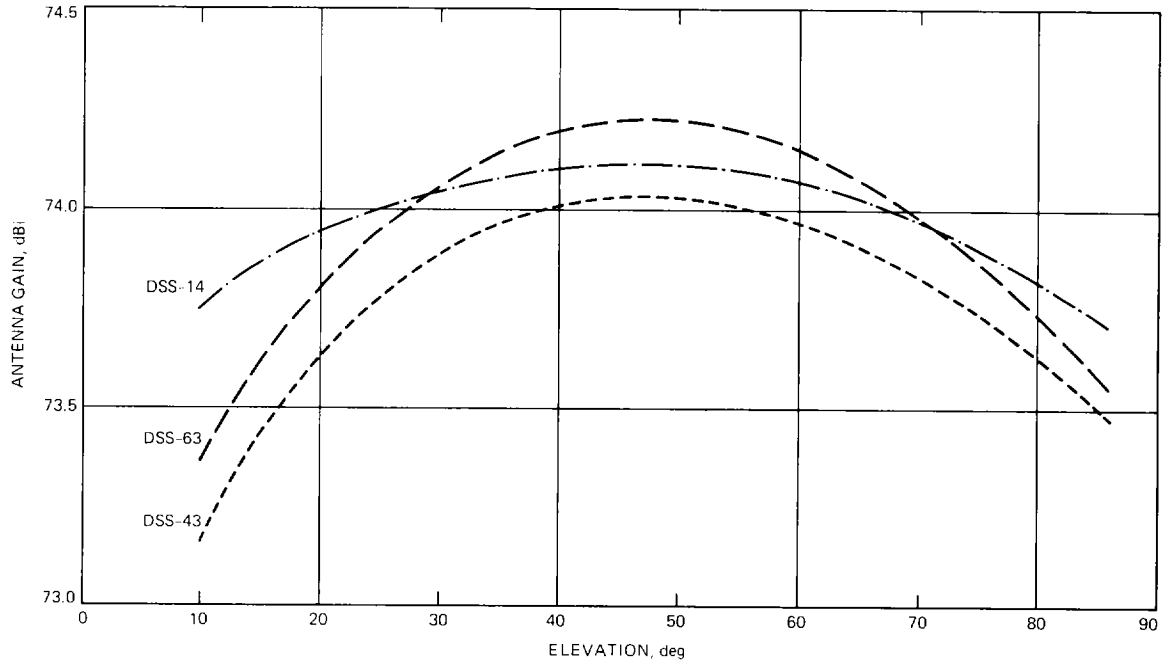

Fig. 7. Calibrated, average X-band gain characteristics for the 70-m antennas, including absorption due to a clear, dry atmosphere.

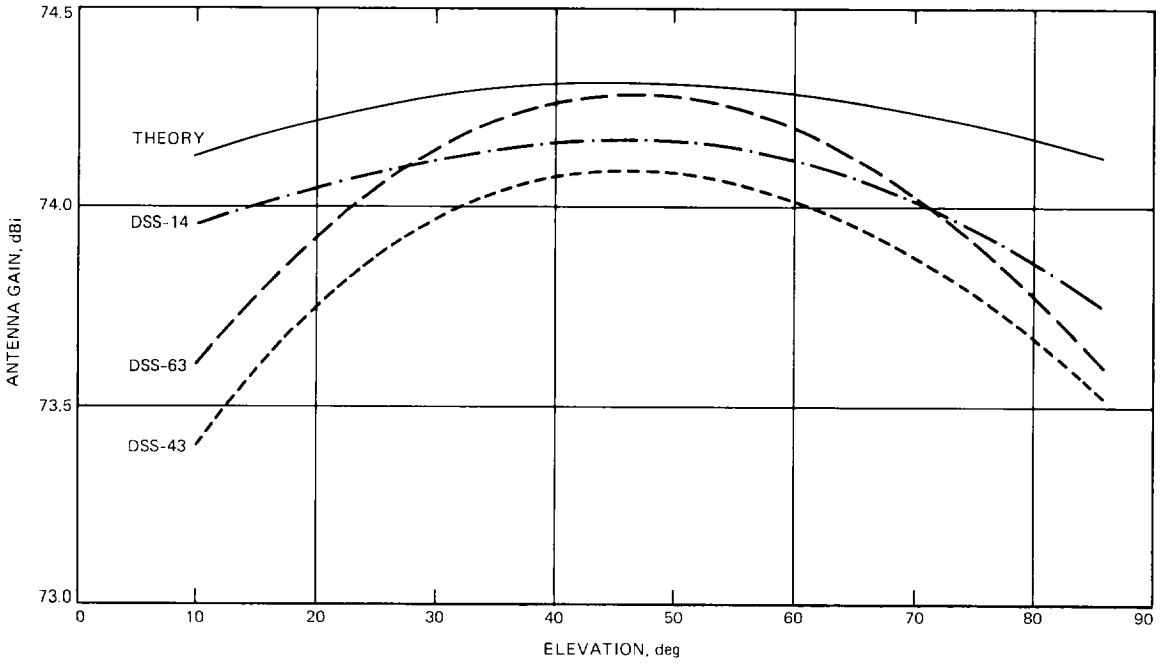

Fig. 8. Calibrated, average X-band gain characteristics for the 70-m antennas; no atmospheric absorption has been included.

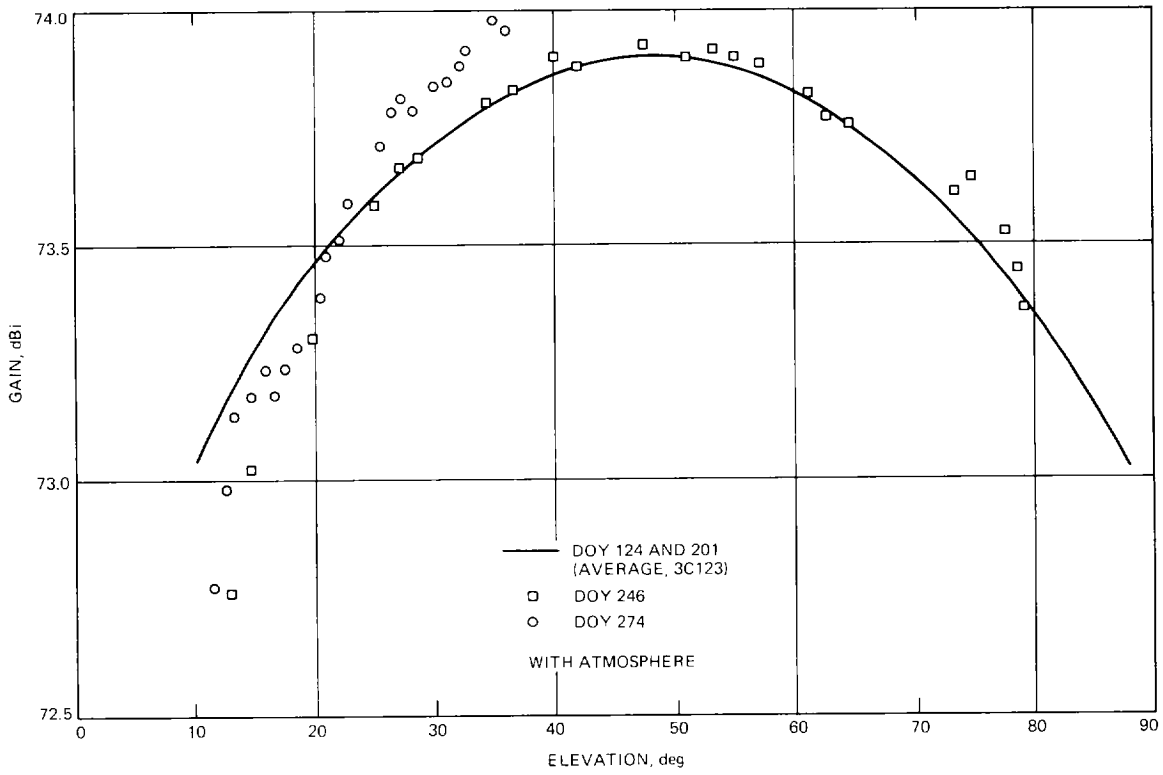

Fig. 9. Comparison of the X-band gain characteristics at DSS-63 before and after rebolting the structural brace.

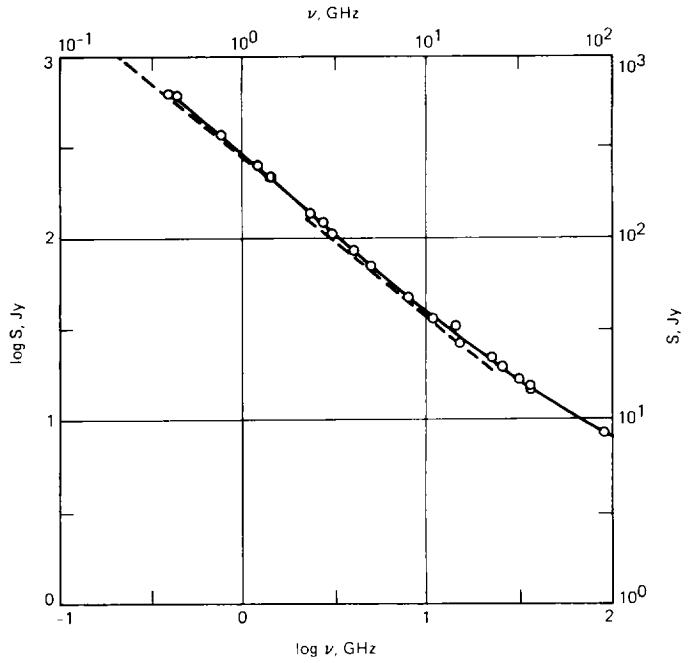

Fig. 10. Flux density spectrum for source 3C274. The points correspond to measured values obtained by various workers, and the solid curve is a cubic power law fit based on equal weighting. The dashed linear curves are estimates based on the artificial-moon calibraton method.

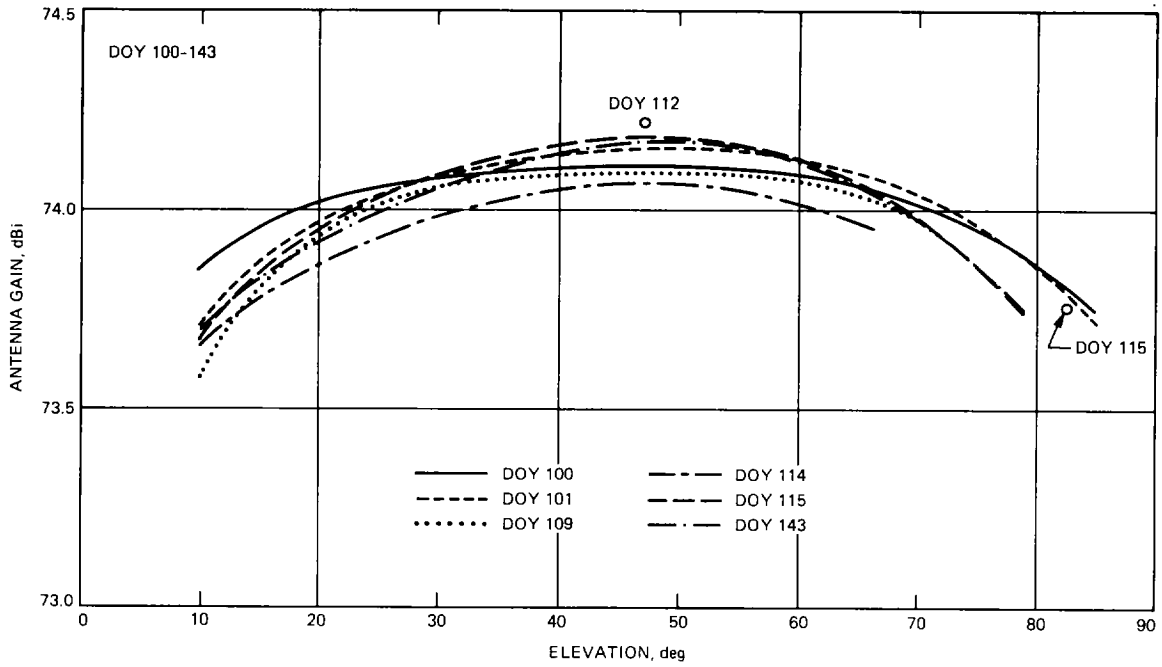

Fig. 11. X-band gain versus elevation for the 70-m antenna at DSS-14 including calibration adjustments and atmospheric absorption.

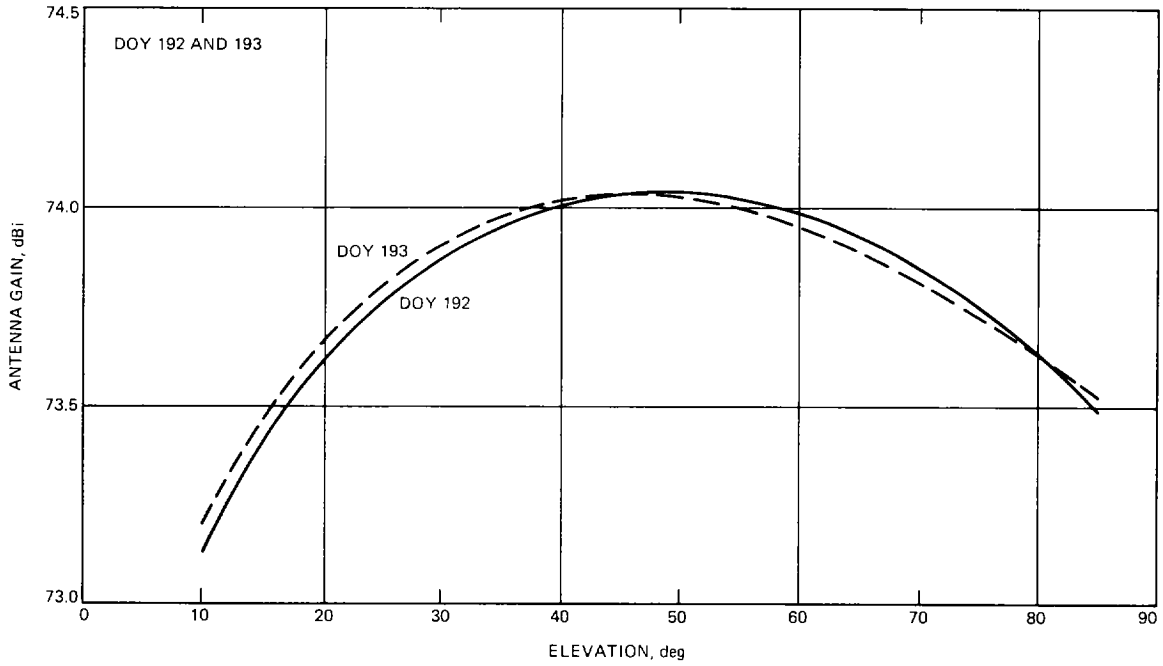

Fig. 12. X-band gain versus elevation for the 70-m antenna at DSS-43 including calibration adjustments and atmospheric absorption.

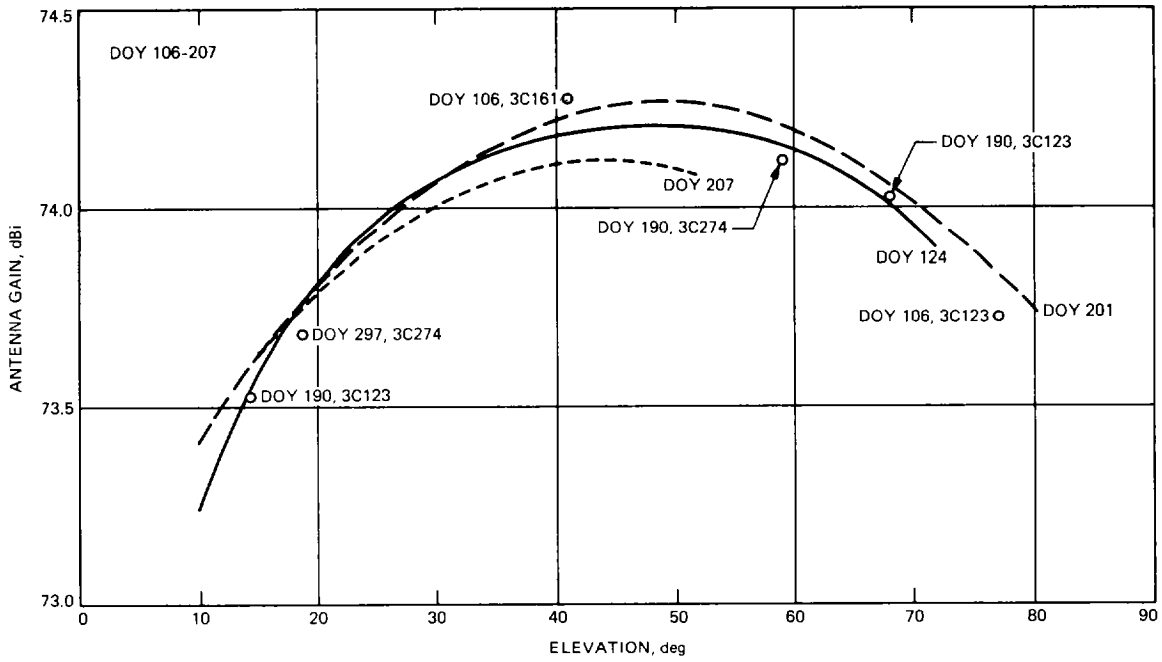

Fig. 13. X-band gain versus elevation for the 70-m antenna at DSS-63 including calibration adjustments and atmospheric absorption.

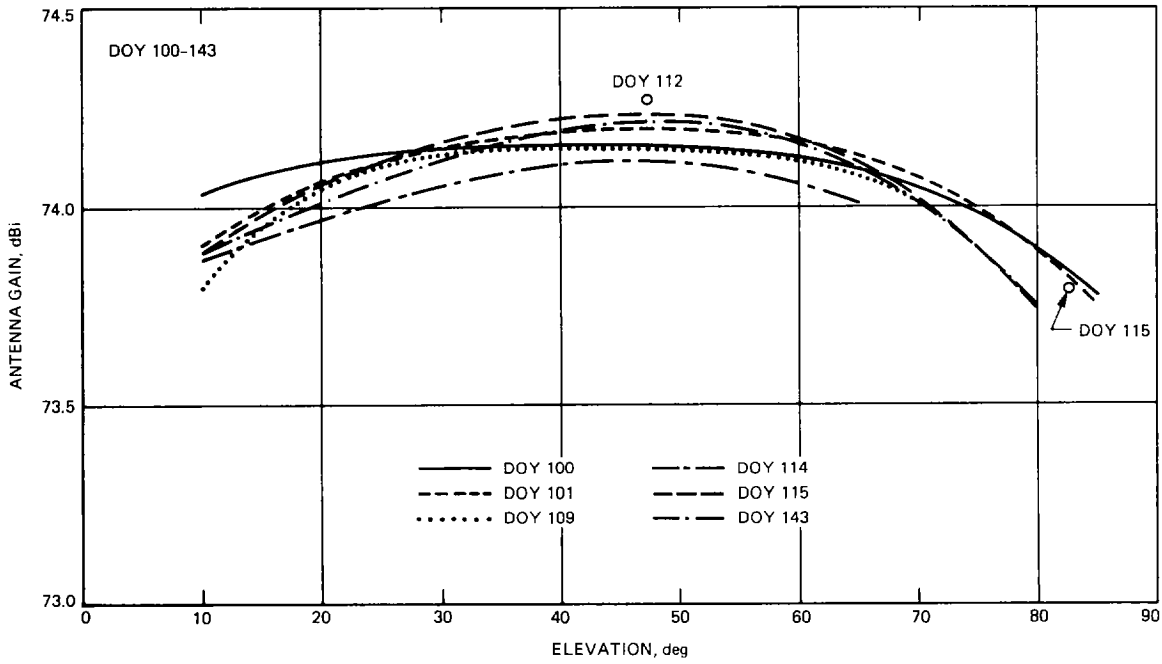

Fig. 14. X-band gain versus elevation for the 70-m antenna at DSS-14 including calibration adjustments; atmospheric absorption has been removed.

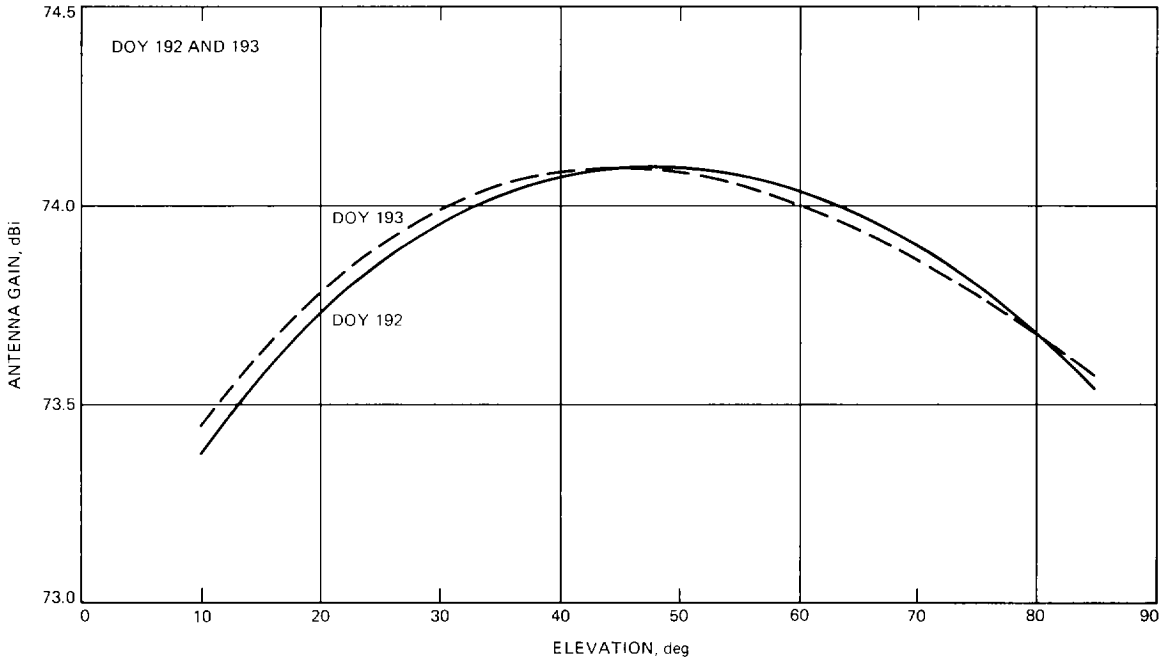

Fig. 15. X-band gain versus elevation for the 70-m antenna at DSS-43 including calibration adjustments; atmospheric absorption has been removed.

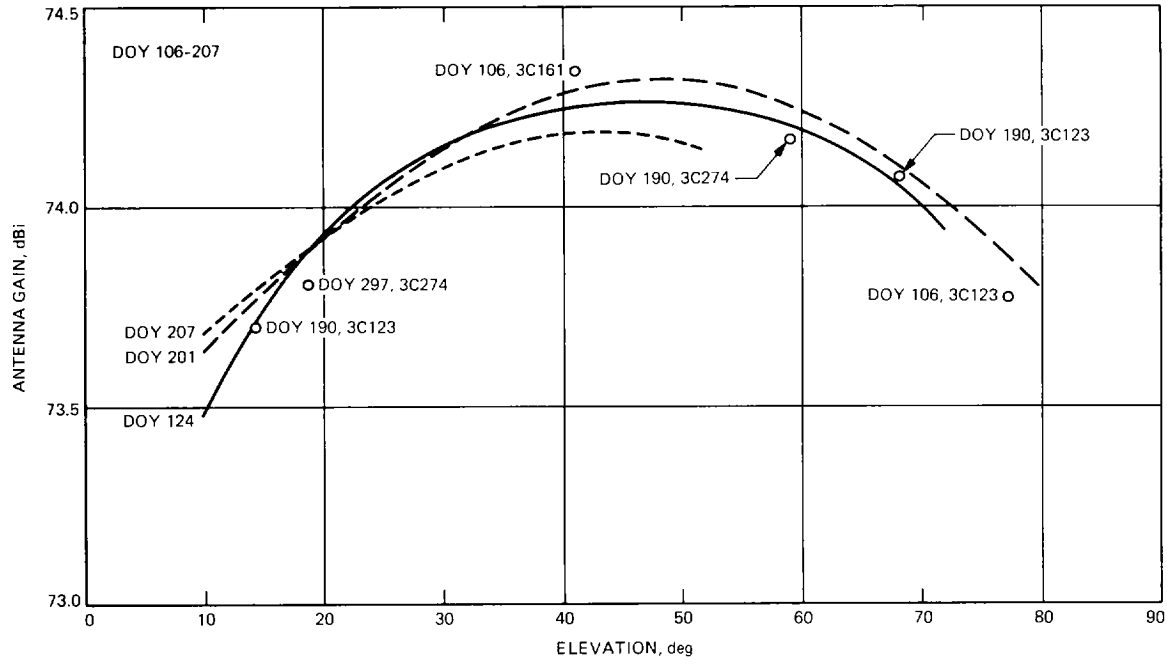

Fig. 16. X-band gain versus elevation for the 70-m antenna at DSS-63 including calibration adjustments; atmospheric absorption has been removed.

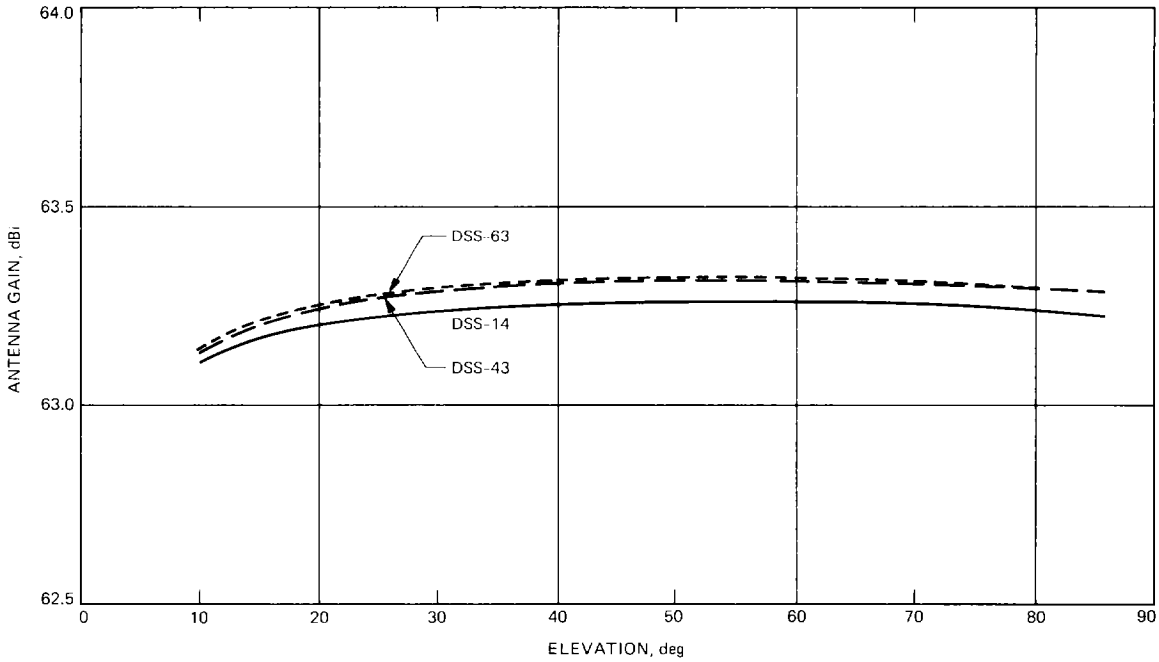

Fig. 17. Calibrated, average S-band gain characteristics for the 70-m antennas at DSS-14 and DSS-43 including absorption due to a clear, dry atmosphere.

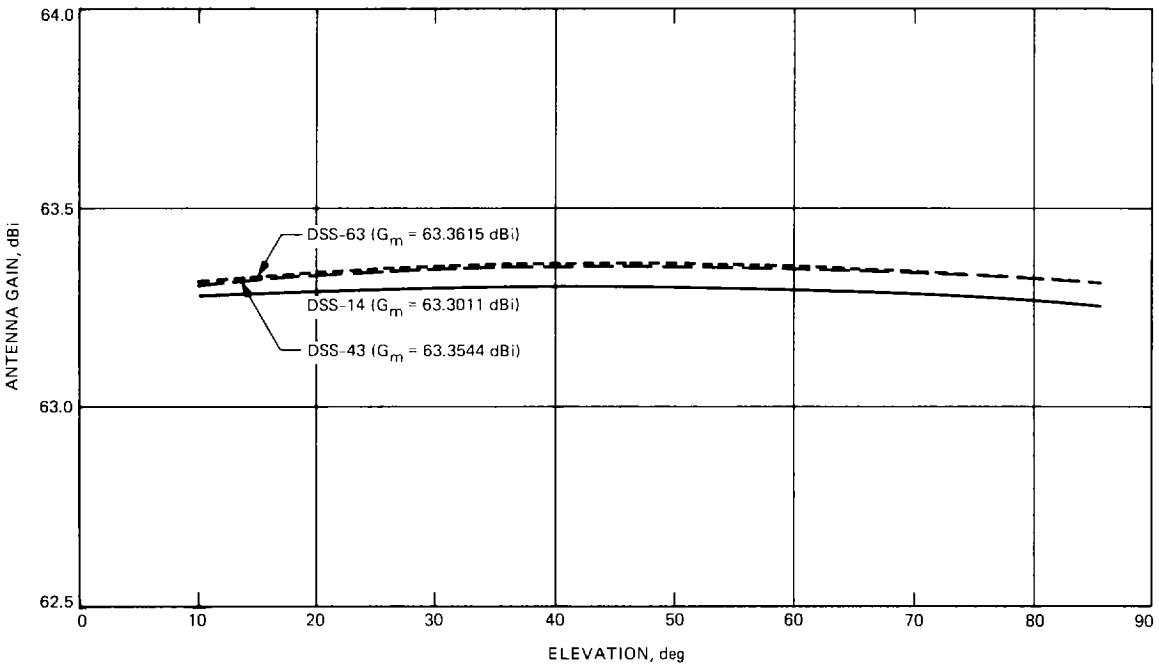

Fig. 18. Calibrated, average S-band gain characteristics for the 70-m antennas at DSS-14 and DSS-43; no atmospheric absorption has been included.

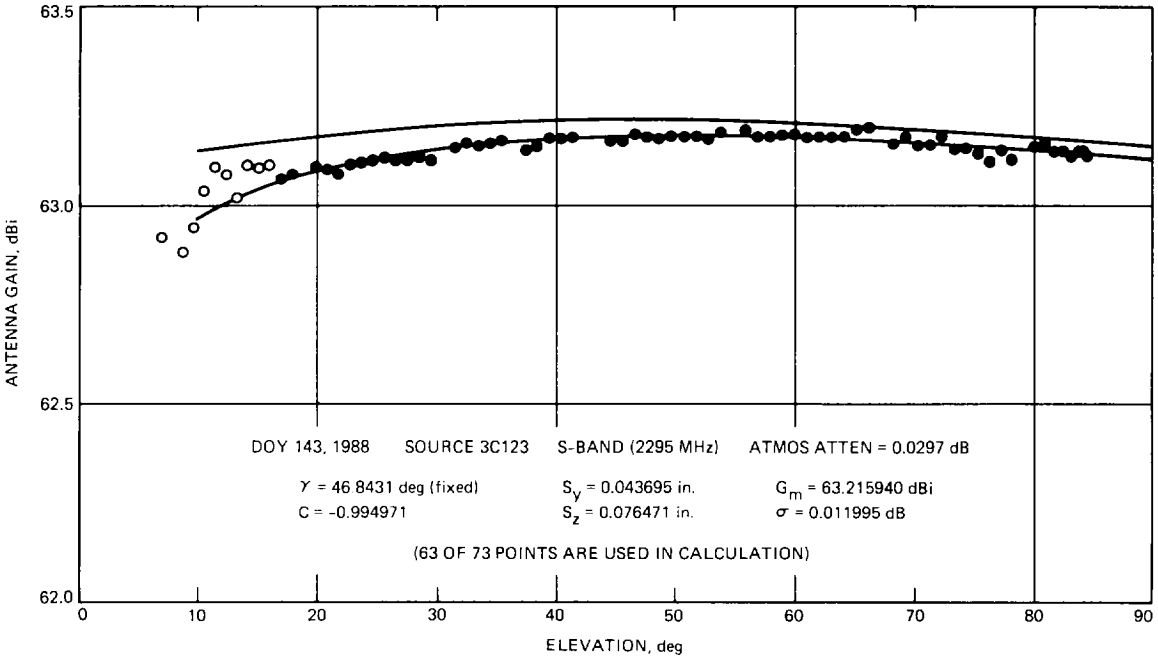

Fig. 19. S-band gain versus elevation for the 70-m antenna at DSS-14 based on uncalibrated data. The lower curve includes atmospheric absorption.

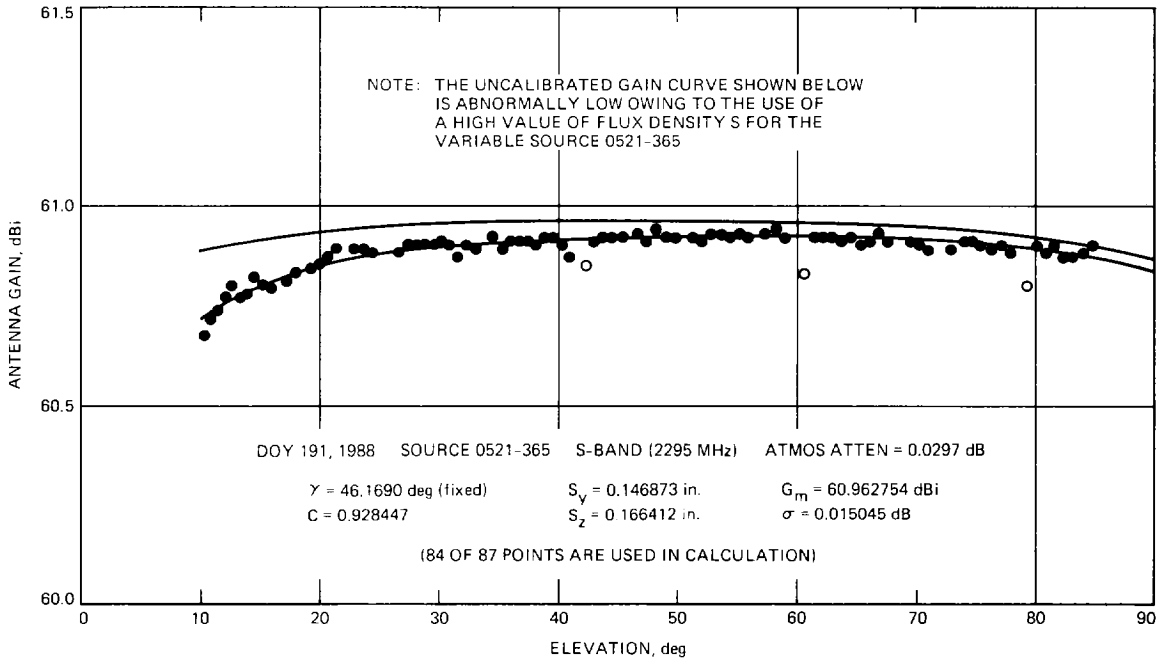

Fig. 20. S-band gain versus elevation for the 70-m antenna at DSS-43 based on uncalibrated data. The lower curve includes atmospheric absorption.

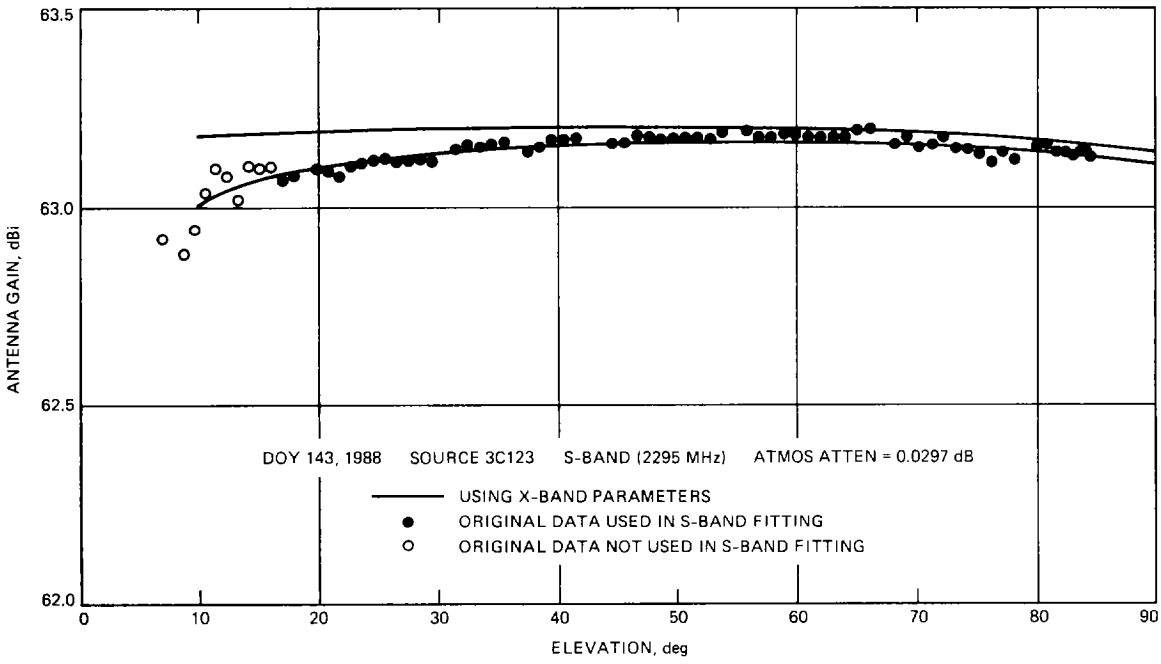

Fig. 21. The same data is presented as in Fig. 19, except that the curve fit is based on the Ruze-Levy parameters obtained at X-band.

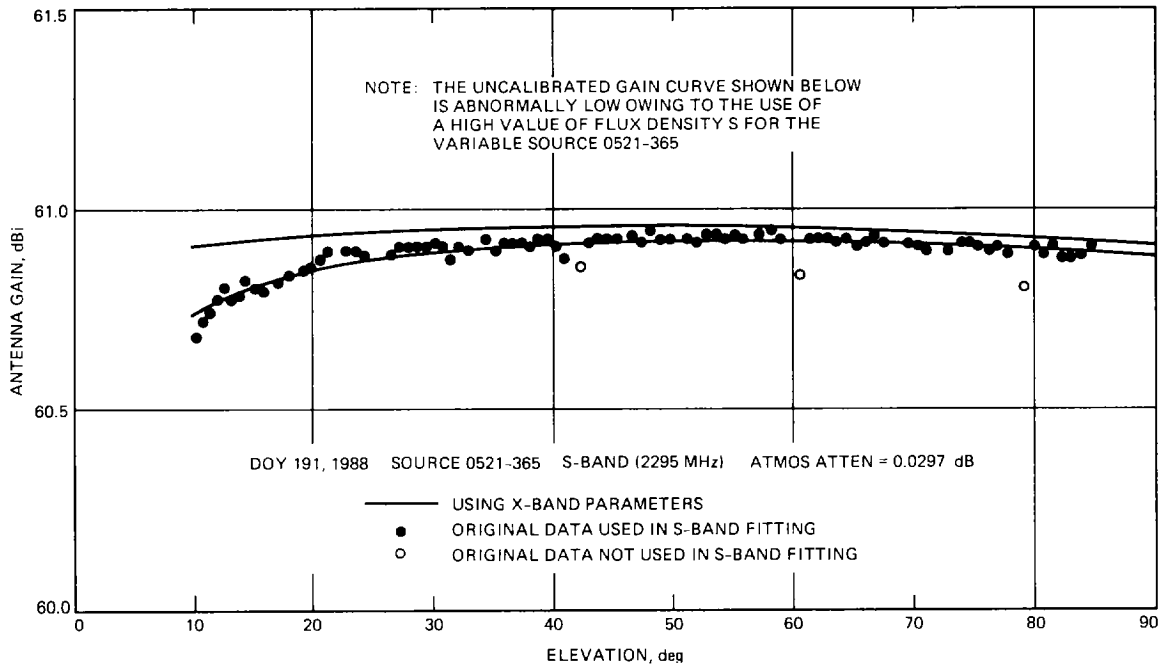

Fig. 22. The same data is presented as in Fig. 20, except that the curve fit is based on the Ruze-Levy parameters obtained at X-band.

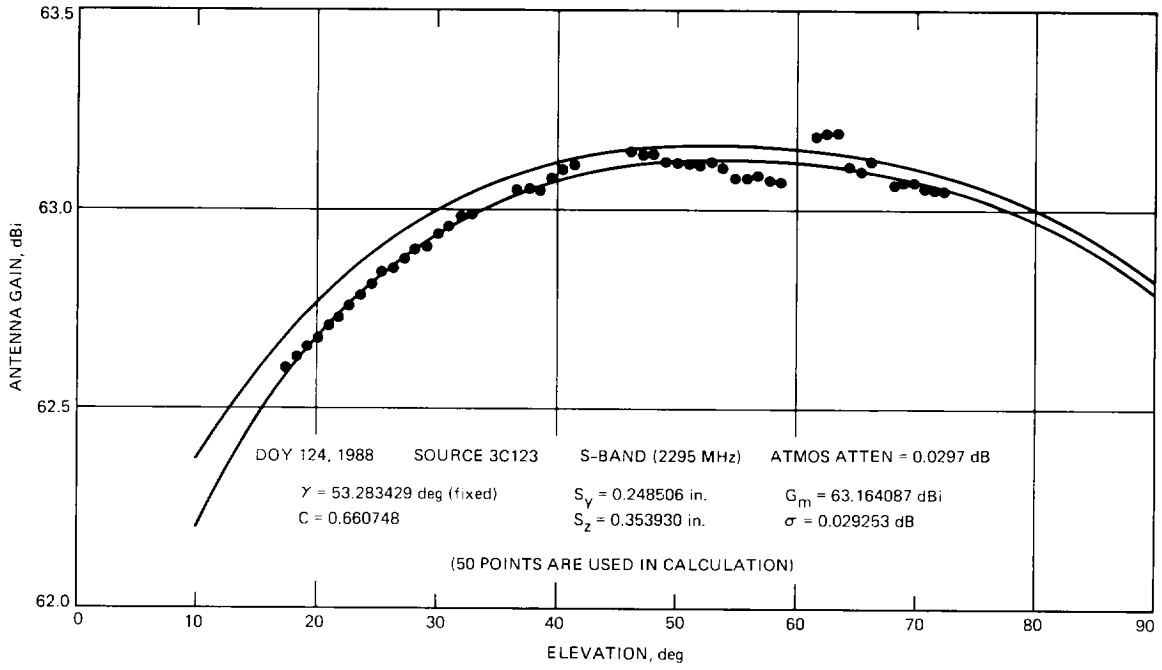

Fig. 23. S-band gain versus elevation for the 70-m antenna at DSS-63 based on uncalibrated data. The lower curve includes atmospheric absorption. A systematic error has caused excessive gain loss at low elevations, but the peak gain is in agreement with measurements at DSS-14 and DSS-43.

Appendix A

Curve Fits to Individual Runs and Stations

The results of curve fitting to the efficiency data from individual runs at DSS-14 (DOY 100–143), DSS-43 (DOY 192–194), and DSS-63 (DOY 124–207) are shown in Figs. A-1–A-3. The data points shown in these figures are the $G(\alpha)$ values computed directly from the $\epsilon(\alpha)$ values measured at each station by means of Eq. (5). The upper curve is the result of fitting to the corresponding $G_0(\alpha)$ values obtained from Eq. (4), and the lower curve is the corresponding $G(\alpha)$ curve obtained from Eq. (4) using the $G_0(\alpha)$ fit. Thus, the upper curve is the best fit to Eq. (3) and represents the antenna performance without atmospheric attenuation, while the lower curve corresponds to the actual performance at the station.

Since the $\epsilon(\alpha)$ values for each station are computed from the measured antenna temperatures $T(\alpha)$ by means of the relationship

$$\epsilon(\alpha) = \frac{T(\alpha)}{T_a} \tag{A-1}$$

where

$$T_a = \frac{T_s}{C_r}$$

$T_s = \dfrac{\pi D^2 S}{8k}$ = 100 percent efficient source temperature for antenna of diameter D

C_r = source-size correction factor

S = source flux density

k = Boltzmann's constant

the gain $G_0(\alpha)$ may be expressed as

$$G_0(\alpha) = \frac{A_{0_z}}{\sin \alpha} + 10 \log T(\alpha) + 10 \log \left(\frac{8\pi k}{\lambda^2}\right) + 10 \log \left(\frac{C_r}{S}\right) \tag{A-2}$$

This explicitly shows that the elevation dependence enters through both the attenuation correction and the measured antenna temperatures $T(\alpha)$, so that the shape of the $G_0(\alpha)$ curve depends to some extent on the value of A_{0_z} chosen. However, the variation in this parameter at a given station is generally less than 0.005 dB for good weather, so that at the lowest elevation for which the model should be used (10 deg) the corresponding error in $G_0(\alpha)$ amounts to less than 0.03 dB. Thus, one can assume that in the absence of systematic errors in the measurement of $T(\alpha)$, the values of γ, G_1, G_2, and G_3 in Eq. (3) should be reasonably accurate.

The maximum gain, G_m, on the other hand, obviously depends directly on the assumed values for the source flux density S and source-size correction factor C_r, and the accuracy of these parameters is discussed in Section IV.

Figures A-4–A-6 show the results of fitting to the combined calibrated data sets for the individual stations as discussed in Section IV.E. The curves shown are those appearing in Fig. 8 (no atmosphere), and it is seen that the rms error of the fits is ~0.03–0.05 dB for all three stations.

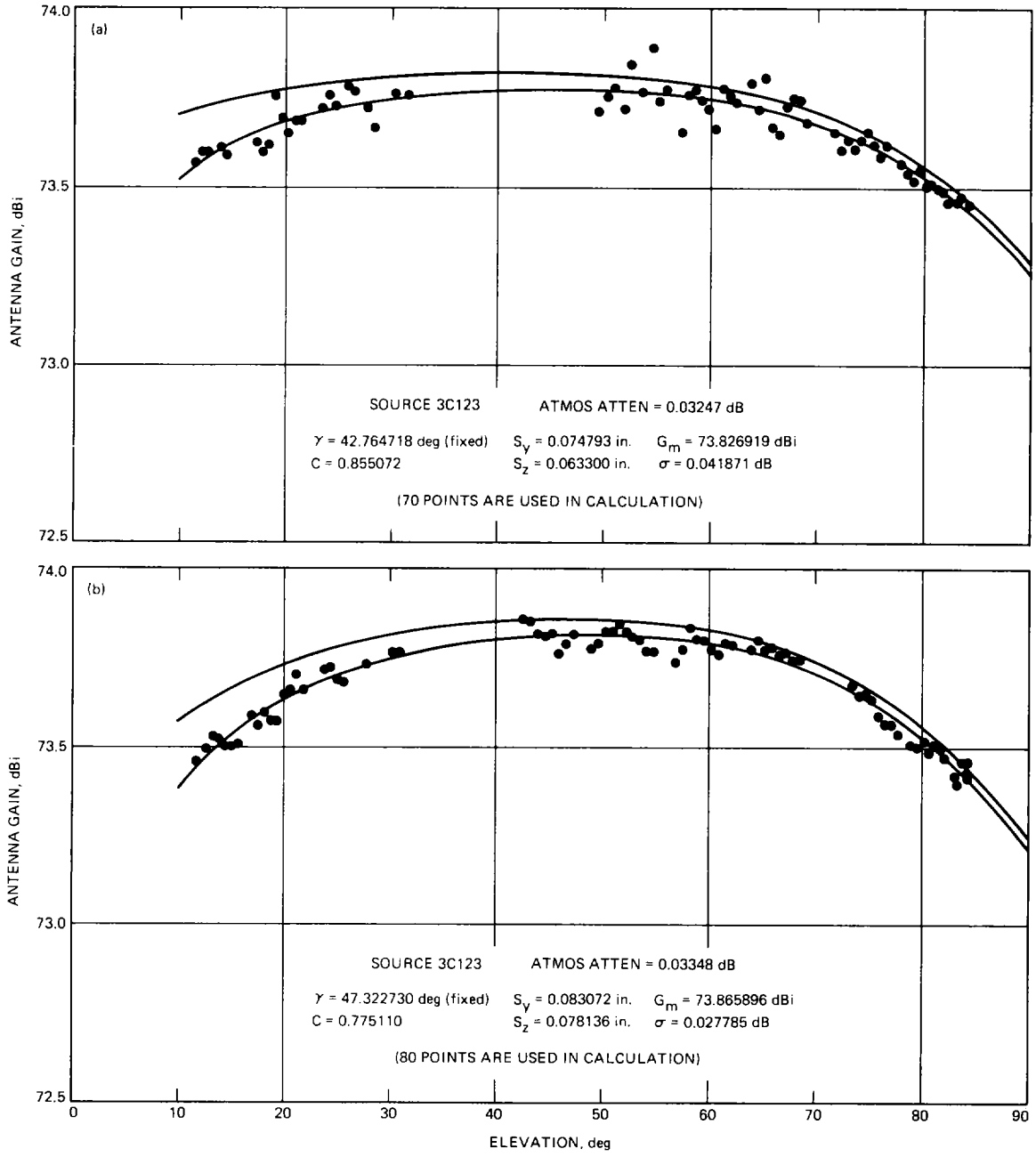

Fig. A-1. Uncalibrated X-band gain versus elevation data for DSS-14 showing Ruze-Levy curve fits for each individual run: (a) DOY 100, (b) DOY 101, (c) DOY 109, (d) DOY 114, (e) DOY 115, and (f) DOY 143. The lower curves include atmospheric absorption.

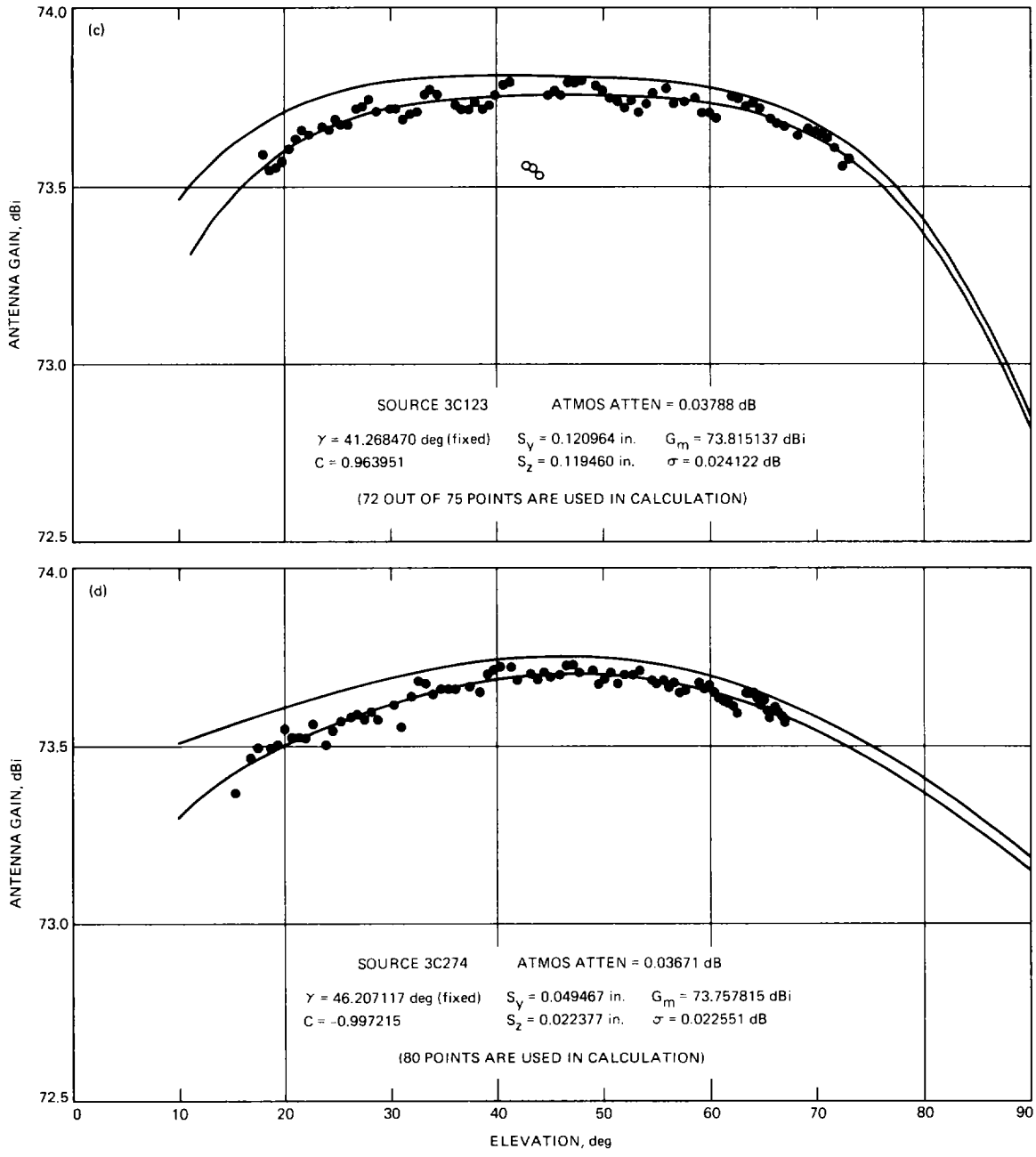
(c)
74.0
73.5
73.0
72.5
ANTENNA GAIN, dBi
SOURCE 3C123
ATMOS ATTEN = 0.03788 dB
Y = 41.268470 deg (fixed)
S_y = 0.120964 in.
G_m = 73.815137 dBi
C = 0.963951
S_z = 0.119460 in.
σ = 0.024122 dB
(72 OUT OF 75 POINTS ARE USED IN CALCULATION)
(d)
74.0
73.5
73.0
72.5
ANTENNA GAIN, dBi
SOURCE 3C274
ATMOS ATTEN = 0.03671 dB
Y = 46.207117 deg (fixed)
S_y = 0.049467 in.
G_m = 73.757815 dBi
C = -0.997215
S_z = 0.022377 in.
σ = 0.022551 dB
(80 POINTS ARE USED IN CALCULATION)
0
10
20
30
40
50
60
70
80
90
ELEVATION, deg

Fig. A-1 (contd)

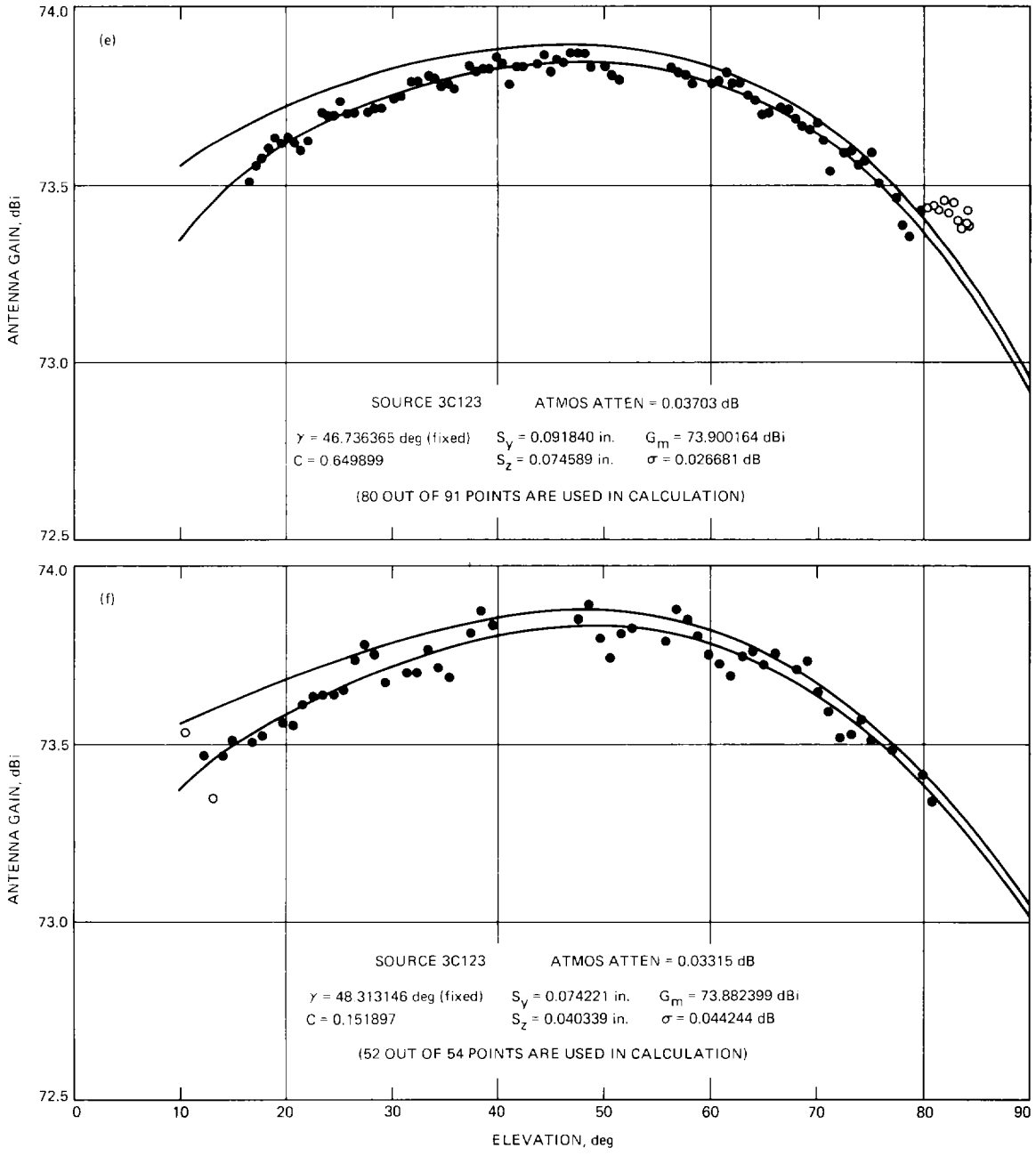
(e)
74.0
73.5
73.0
72.5
ANTENNA GAIN, dBi
SOURCE 3C123 ATMOS ATTEN = 0.03703 dB
γ = 46.736365 deg (fixed) S_y = 0.091840 in. G_m = 73.900164 dBi
C = 0.649899 S_z = 0.074589 in. σ = 0.026681 dB
(80 OUT OF 91 POINTS ARE USED IN CALCULATION)
(f)
74.0
73.5
73.0
72.5
ANTENNA GAIN, dBi
SOURCE 3C123 ATMOS ATTEN = 0.03315 dB
γ = 48.313146 deg (fixed) S_y = 0.074221 in. G_m = 73.882399 dBi
C = 0.151897 S_z = 0.040339 in. σ = 0.044244 dB
(52 OUT OF 54 POINTS ARE USED IN CALCULATION)
0
10
20
30
40
50
60
70
80
90
ELEVATION, deg

Fig A-1 (contd)

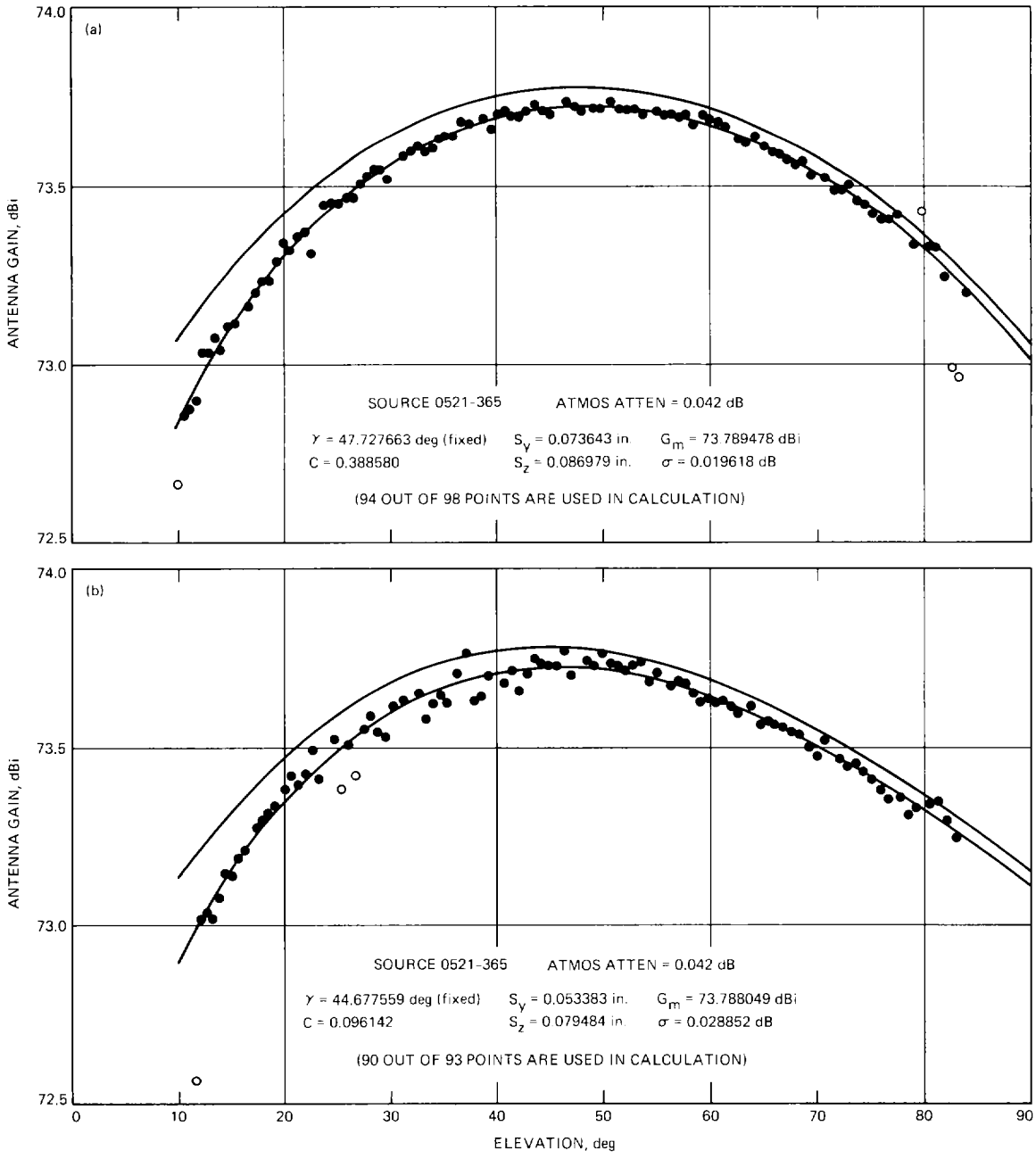

Fig. A-2. Uncalibrated X-band gain versus elevation data for DSS-43 showing Ruze-Levy curve fits for each individual run: (a) DOY 192; (b) DOY 193; (c) DOY 193; and (d) DOY 194. The lower curves (or data points) include atmospheric absorption.

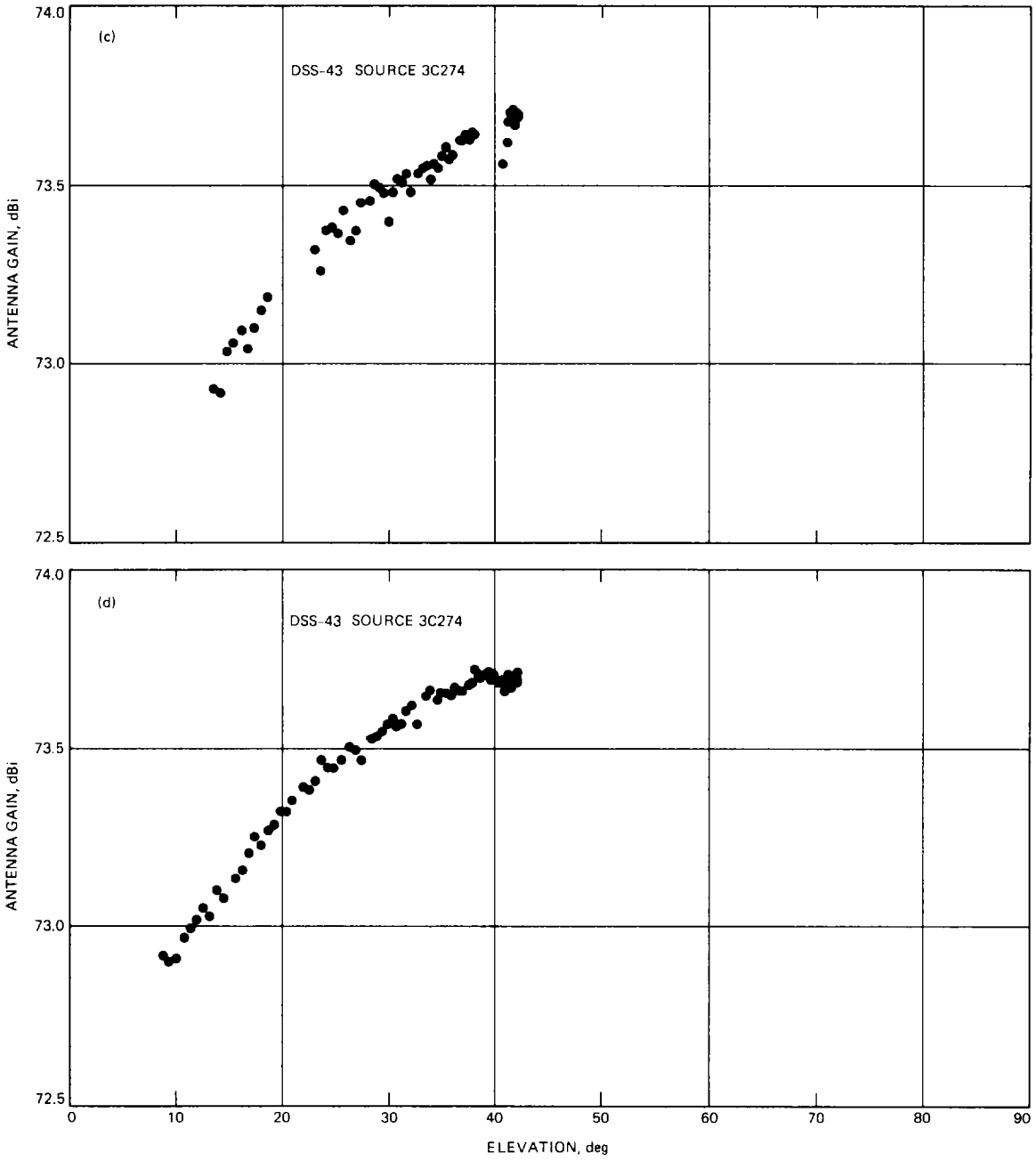
(c)
DSS-43 SOURCE 3C274
ANTENNA GAIN, dBi
74.0
73.5
73.0
72.5
(d)
DSS-43 SOURCE 3C274
ANTENNA GAIN, dBi
74.0
73.5
73.0
72.5
0
10
20
30
40
50
60
70
80
90
ELEVATION, deg

Fig. A-2 (contd)

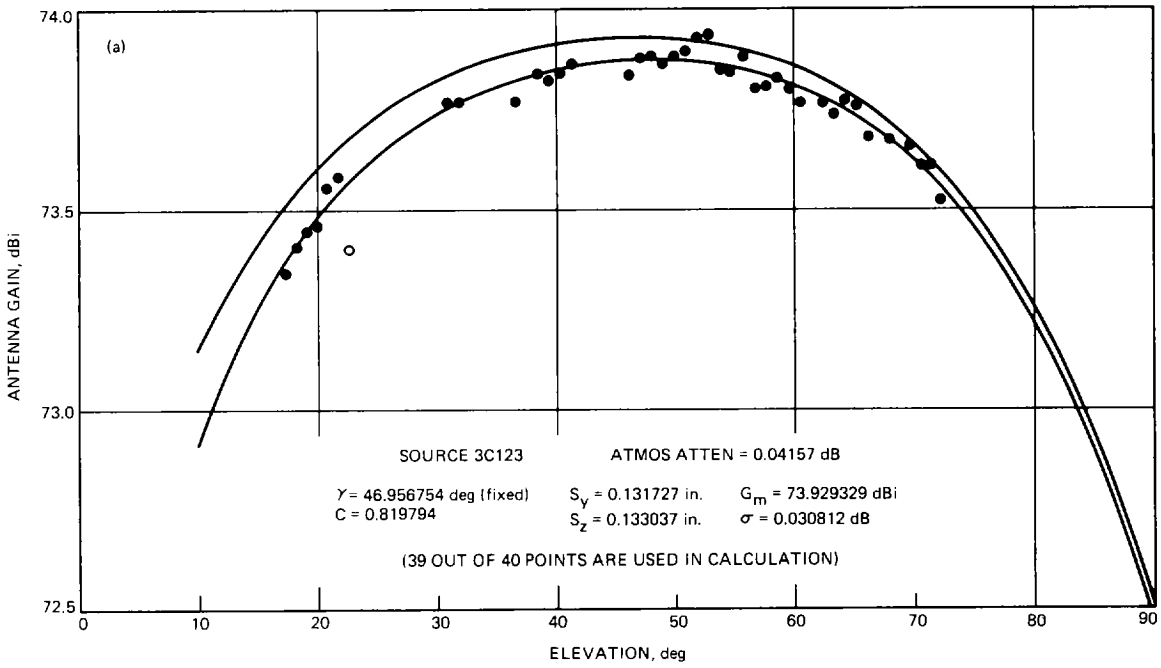

Fig. A-3. Uncalibrated X-band gain versus elevation data for DSS-63 showing Ruze-Levy curve fits for each individual run: (a) DOY 124, (b) DOY 201, and (c) DOY 207. The lower curves include atmospheric absorption.

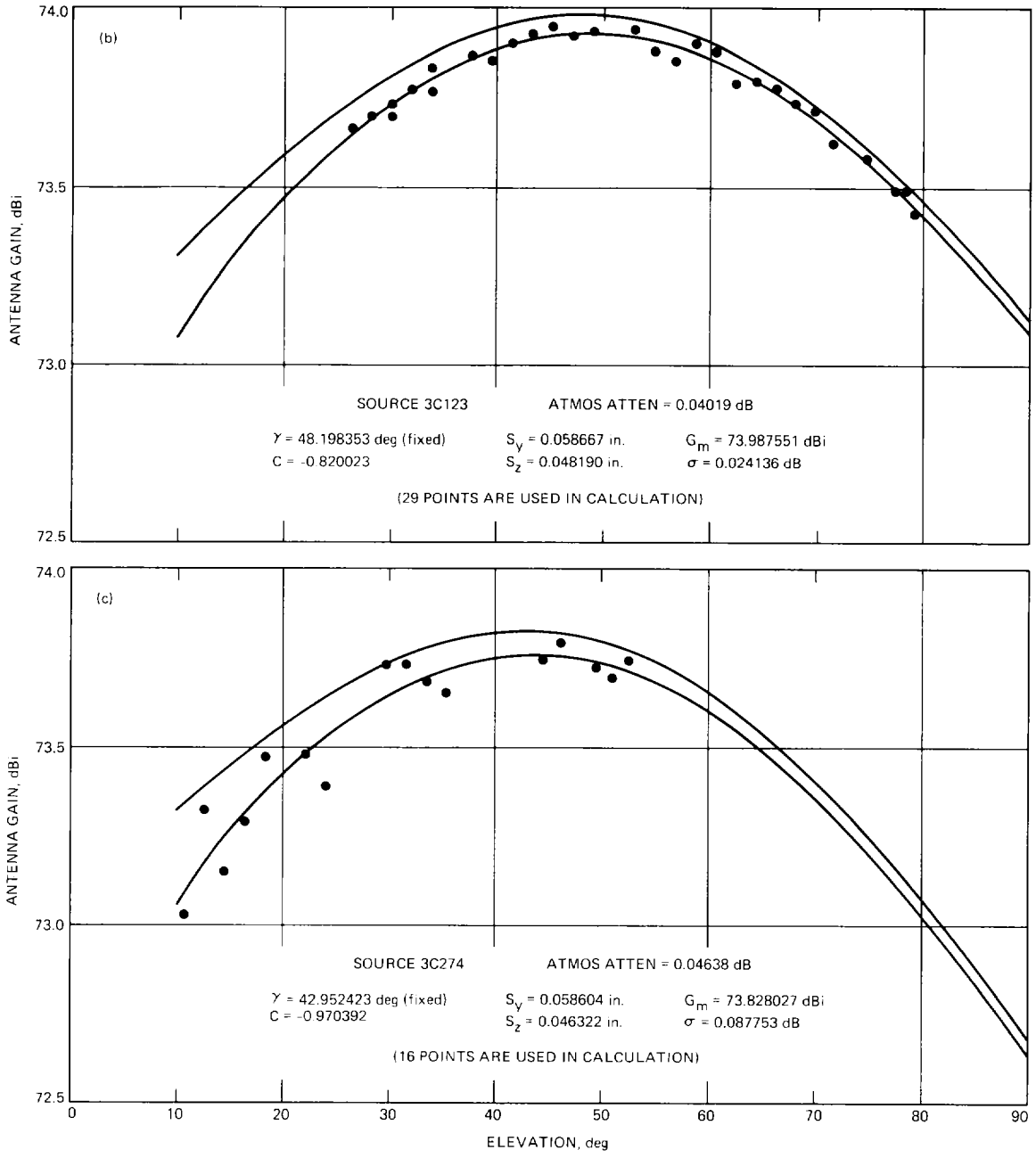
(b)
74.0
73.5
73.0
72.5
ANTENNA GAIN, dBi
SOURCE 3C123
ATMOS ATTEN = 0.04019 dB
Y = 48.198353 deg (fixed)
C = -0.820023
S_y = 0.058667 in.
S_z = 0.048190 in.
G_m = 73.987551 dBi
σ = 0.024136 dB
(29 POINTS ARE USED IN CALCULATION)
(c)
74.0
73.5
73.0
72.5
ANTENNA GAIN, dBi
SOURCE 3C274
ATMOS ATTEN = 0.04638 dB
Y = 42.952423 deg (fixed)
C = -0.970392
S_y = 0.058604 in.
S_z = 0.046322 in.
G_m = 73.828027 dBi
σ = 0.087753 dB
(16 POINTS ARE USED IN CALCULATION)
0
10
20
30
40
50
60
70
80
90
ELEVATION, deg

Fig. A-3 (contd)

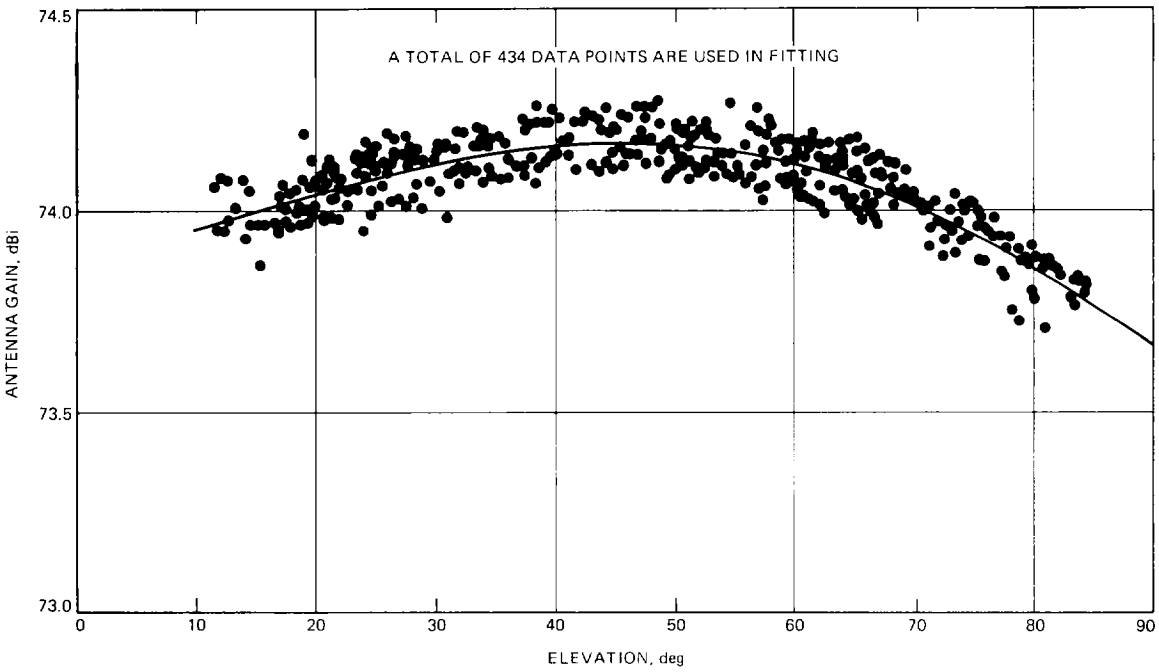

Fig. A-4. Ruze-Levy curve fits to the combined, calibrated data for DSS-14 (no atmospheric absorption).

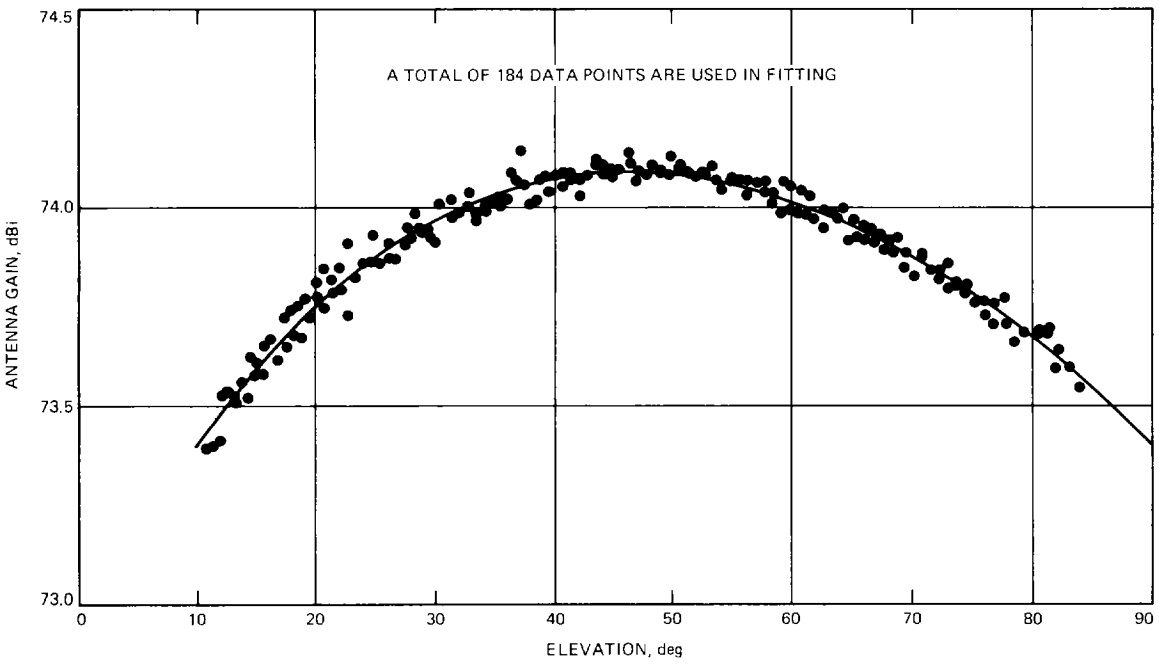

Fig. A-5. Ruze-Levy curve fits to the combined, calibrated data for DSS-43 (no atmospheric absorption).

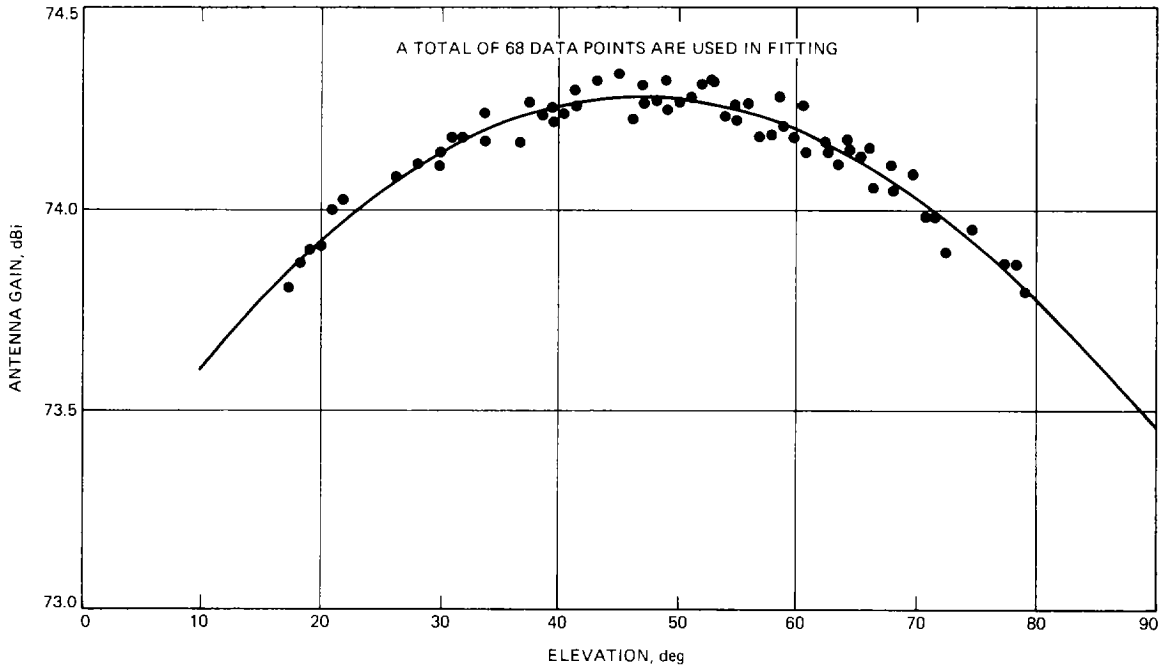

Fig. A-6. Ruze-Levy curve fits to the combined, calibrated data for DSS-63 (no atmospheric absorption).

Appendix B

Periodic Measurement Errors and Systematic Offsets

I. Periodic Errors

Measurements made at DSS-14 show distinctive systematic errors, the most pronounced example of which is found in the data for DOY 109, which show a periodic fluctuation superimposed on the $\epsilon(\alpha)$ curve (see Fig. A-1c). This is most clearly seen over the range 26 deg $< \alpha <$ 60 deg, but appears to persist to some degree over the entire range of elevation angles at which measurements were made. Also, there is an indication of the same behavior in the data obtained on other days at this station.

Analysis of the DOY 109 data also reveals a similar periodicity in the pointing coefficient C_p. The two effects are compared in Fig. B-1 where $C_p - 1$ and ϵ are each plotted as a function of elevation angle α for the range 26 deg $< \alpha <$ 42 deg. It can be seen that not only do each of these show a periodic behavior, but that the two show a strong correlation as well. If a linear trend $\bar{\epsilon}(\alpha)$ is subtracted from the $\epsilon(\alpha)$ data, then the correlation between $C_p - 1$ and $\epsilon - \bar{\epsilon}$ appears as shown in Fig. B-2. The correlation coefficient is found to be $r = -0.581$, which corresponds to a probability that the two quantities are uncorrelated of ~0.006. The correlation is furthermore seen to be negative, as would be the case if there were a causal relationship between the pointing coefficient and measured efficiency, i.e., if the measured temperature $T(\alpha)$ were reduced as the result of a pointing error.

Since these data were obtained with the APCAL program operating in closed-loop mode, the pointing coefficient has not actually been used to correct the ϵ values.[1] However, one may determine the extent to which the periodic pointing offset shown in Fig. B-1 contributes to the observed periodic efficiency loss shown in the same figure by comparing the sinusoidal curve fit to the efficiency data with the correlation between efficiency and pointing coefficient.

The least squares sinusoidal fit has the form

$$\epsilon - \bar{\epsilon} = C \cos(k\alpha + \phi) \tag{B-1}$$

with $C = 4.0149 \times 10^{-3}$, $k = 54.750$, and $\phi = 88.9$ deg, while the linear correlation is of the form

$$\epsilon - \bar{\epsilon} = a - b(C_p - 1) \tag{B-2}$$

with $a = 2.9305 \times 10^{-3}$ and $b = 0.5752$.

The efficiency and pointing coefficient are related to one another by the equation

$$\epsilon = \frac{\epsilon_m}{C_p} \tag{B-3}$$

where ϵ_m is the value of ϵ for perfect pointing ($C_p = 1$). If a linear approximation is made to this hyperbolic relation for $C_p \geq 1$,

$$\epsilon - \bar{\epsilon} = (\epsilon_m - \bar{\epsilon}) - \epsilon_m(C_p - 1) \tag{B-4}$$

From Eq. (B-1), $\epsilon_m - \bar{\epsilon} = C$, and taking $\epsilon_m = 0.626$ from the original data (average maximum gain for 26 deg $< \alpha <$ 42 deg), the results of the linear correlation, Eq. (B-2), may be compared with the theoretical relationship, Eq. (B-4). This is done in Fig. B-2, where it is seen that the two are very close, thus implying that the observed periodic variation in efficiency has been caused by a periodic pointing error.

The periodic pointing error is thus seen to be of the form

$$C_p - 1 = \frac{C}{\epsilon_m}[1 - \cos(k\alpha + \phi)] \tag{B-5}$$

where $C/\epsilon_m = 4.414 \times 10^{-3}$, which gives a consistent fit to the data of Fig. B-2. In terms of the pointing offset angle $\Delta\Phi$,

$$C_p = \exp\left[4 \ln 2 \left(\frac{\Delta\Phi}{\Phi_B}\right)^2\right] \tag{B-6}$$

where Φ_B = HPBW = 0.030 deg for the 70-m antennas. Thus, expanding the above

$$C_p - 1 \simeq 4 \ln 2 \left(\frac{\Delta\Phi}{\Phi_B}\right)^2 \tag{B-7}$$

from which the maximum offset corresponding to $C_p - 1 = 4.414 \times 10^{-3}$ is $\Delta\Phi = 1.2 \times 10^{-3}$ deg.

[1] G. Milford and J. Horter, *APCAL Technical Manual (Preliminary)*, JPL internal document, Jet Propulsion Laboratory, Pasadena, California, p. 27, May 1988.

In considering the periodic behavior above, the elevation angle α has been treated as the variable. For the range of elevations considered there is a nearly linear relationship between the elevation angle and Greenwich Mean Time (GMT) so that a simple transformation can be made to time as a variable. This leads to the time equivalent of Eq. (B-1),

$$\epsilon - \bar{\epsilon} = C \cos(\omega t + \phi) \tag{B-8}$$

where it is found that $\omega = 11.6871$ deg/hr, giving a period for the oscillation of $T = 0.5626$ hr = 33 min 45 sec.

If a different interval is chosen for the analysis, then similar results are found but with somewhat different values for the fitting parameters. For example, for 44 deg $< \alpha <$ 61 deg, $C = 3.6670 \times 10^{-3}$, $k = 43.8613$, $\phi = -38.2655$ deg, and transforming to a time variable here, $\omega = 12.2083$ deg/hr, giving a period $T = 0.6723$ hr = 40 min 20 sec. Also, for this interval there is no identifiable periodicity in the pointing coefficient, and the correlation between $\epsilon - \bar{\epsilon}$ and $C_p - 1$ is random, thus indicating that either a dominant random component has been added to the pointing coefficient data, or the periodicity in $\epsilon(\alpha)$ is of a different origin here, which seems less likely.

The above analysis leads to the conclusion that the efficiency data for this run have likely been systematically reduced due to pointing errors so that the true efficiency values are given by $\epsilon_m(\alpha) = \epsilon(\alpha) + C$, where $\epsilon(\alpha)$ is the value obtained from the curve fitting procedure discussed in Section III.A. Expressed in terms of gain, this corresponds to taking the curve fits obtained and increasing them by approximately 0.028 dB.

Although the periodic variation in $\epsilon(\alpha)$ is clearly discernible in all of the DSS-14 data, its correlation with the computed pointing coefficient is not, so that in spite of the implication of the above analysis based on the DOY 109 data, there does not appear to be enough evidence to support a general conclusion that pointing errors have contributed 0.028 dB of loss to all, or even most of the DSS-14 gain measurements. In view of this, it seems prudent to treat the above as a probable error and include it in the overall error budget as discussed in Section IV.F.

II. Systematic Offsets

Efficiency data obtained at DSS-63 on DOY 201 show an interesting kind of hysteresis effect. The source, 3C123, was tracked in elevation from 26.34 deg to a maximum value of 79.36 deg, and then back down again to $\alpha = 66.02$ deg, thus providing an overlap of measurements over the range 66 deg $< \alpha <$ 76 deg.

Figure B-3 shows the efficiency data plotted versus elevation for this limited range, and it can be seen from this that the data obtained while the source was setting are consistently below that obtained when it was rising, the difference corresponding to some 0.07 dB.

In this case it appears that at least a partial explanation for the change may be found in the environmental data accompanying the run, according to which the only significant change that occurred was in wind velocity. The sky was clear throughout the entire run, and temperature, pressure, and relative humidity all remained quite stable as well. However, the wind velocity was reported as zero throughout most of the run but picked up to10 mph (SW) sometime between GMT = 0812 and 0927, i.e., exactly when the change in efficiency appears to have taken place.

The situation is summarized in Fig. B-4, in which the efficiency and elevation angle are both plotted in terms of GMT, and the last notation of zero wind velocity (GMT = 0812) and the first entry of 10 mph (SW) wind velocity (GMT = 0927) are shown. It can be seen from this that approximately 50 minutes elapsed between the reading taken at maximum elevation (GMT = 085455) and the first reading taken as the source was setting (GMT = 094505), and that the former was also probably depressed as a result of wind, i.e., the wind may have actually picked up shortly before GMT = 0900.

As a check on this, the gain loss versus wind velocity data from 810-5 rev. D[2] for the 70-m antennas have been considered. Extrapolation of these data down to 10 mph results in a predicted gain loss of 0.034 dB. Since the 810-5 data represent the worst case attitude condition for gain loss resulting from wind-induced distortion, it appears that wind alone cannot account for the 0.07 dB loss shown in Fig. B-3.[3]

Another example of a systematic offset is provided by the data from DSS-14 on DOY 115 and 116. This run was begun when the source was rising and very close to its maximum altitude. Data were collected as it rose to its maximum altitude and then proceeded to set, covering the range of elevations from 84.23 deg down to 16.56 deg. However, the entire set of measurements, including both rising and setting, for $\alpha \geqslant 80.30$ deg shows a systematic offset amounting to $\Delta G = 0.12$ dB (see Fig. A-1d). No explanation for this can be found in the data provided with the report.

---

[2] *Deep Space Network/Flight Project Interface Design Handbook, Vol I: Existing DSN Capabilities, Vol. II: Proposed DSN Capabilities*, JPL 810-5, rev. D (internal documents), TCI-10, rev. D, Table 3, July 15, 1988 (Vol. I), November 1, 1986 (Vol. II).

[3] Roy Levy, personal communication.

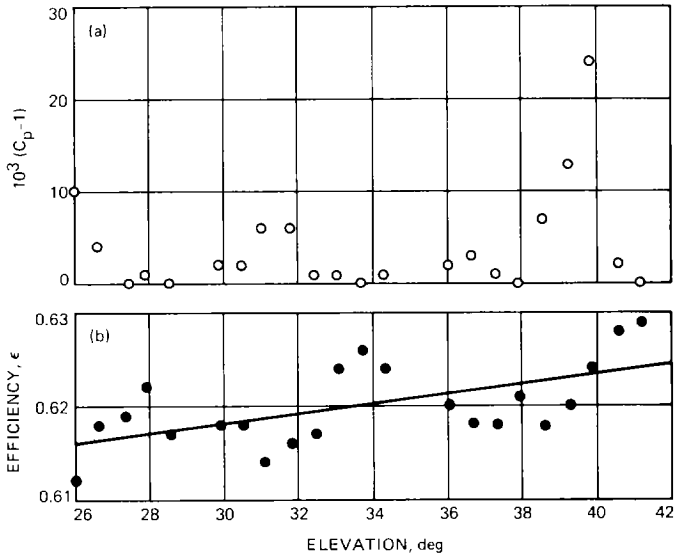

Fig. B-1. A comparison of X-band (a) pointing coefficient and (b) efficiency for DSS-14, DOY 109, showing correlation between the two quantities.

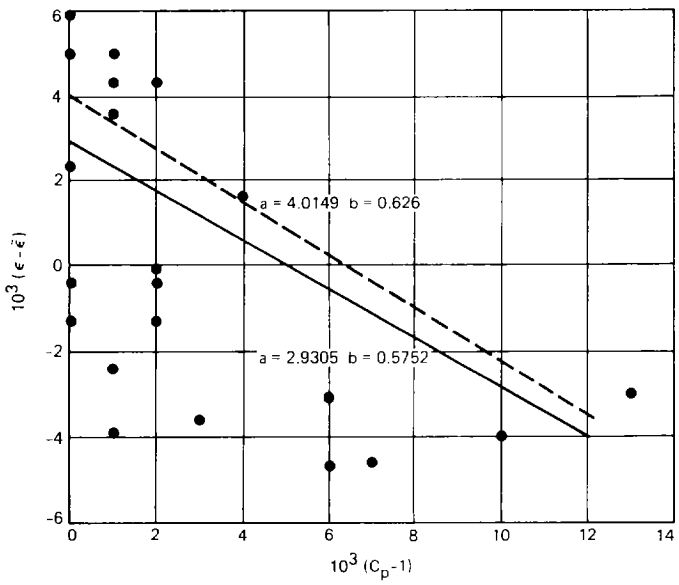

Fig. B-2. Correlation diagram for X-band efficiency versus pointing coefficient for DSS-14, DOY 109. The solid line is the linear regression curve for the data, and the dashed line corresponds to prediction based on a causal relationship between the two quantities.

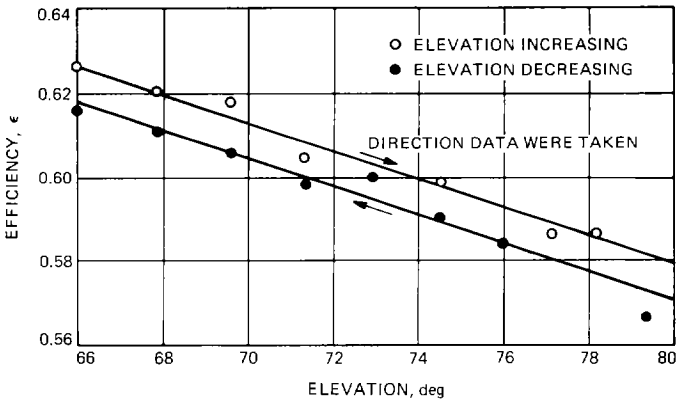

Fig. B-3. Comparison of the X-band efficiency curves obtained at DSS-63, DOY 201, for increasing and decreasing elevation. The approximately 0.07-dB difference is partially explained on the basis of a time-dependent wind-loading effect.

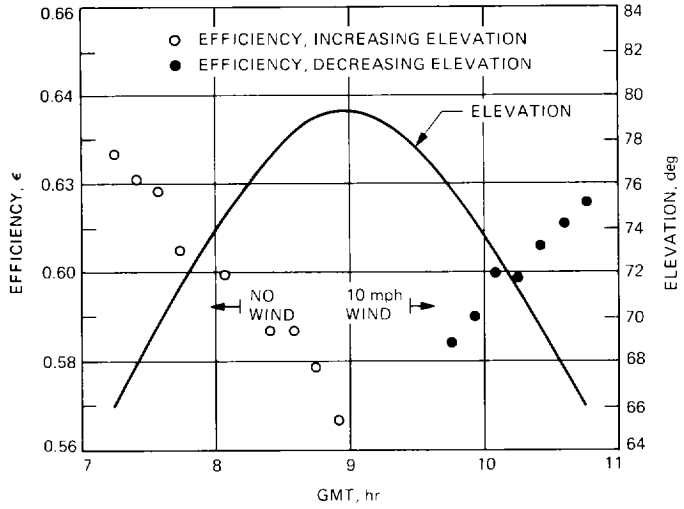

Fig. B-4. X-band efficiency and elevation angle versus GMT for DSS-63, DOY 201, showing the onset of a 10-mph (SW) wind between the rising and setting curves.